Ferroelectric, dielectric and piezoelectric properties of ferroelectric thin films and ceramics

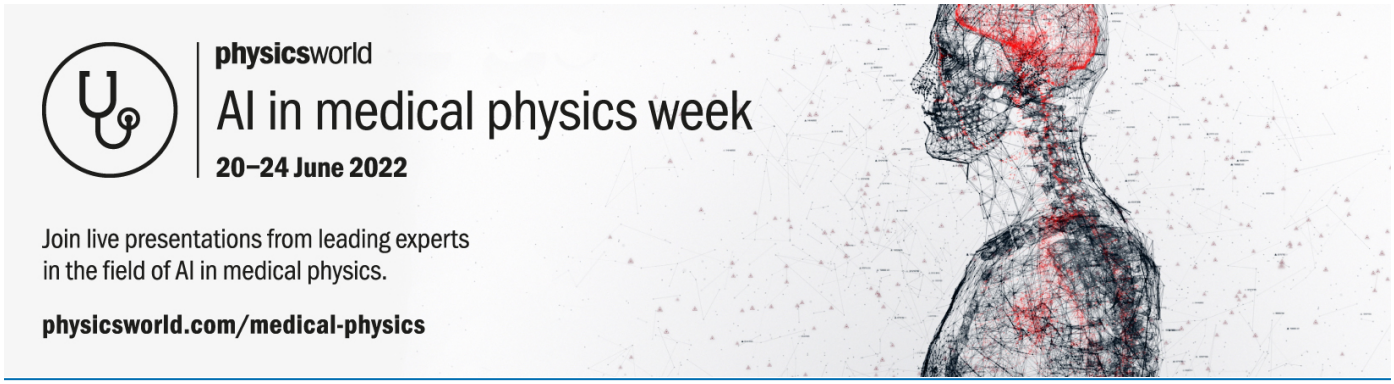

Rep. Prog. Phys. **61** (1998) 1267–1324. Printed in the UK PII: S0034-4885(98)90105-1

Ferroelectric, dielectric and piezoelectric properties of ferroelectric thin films and ceramics

Dragan Damjanovic

Laboratory of Ceramics, Department of Materials Science, Swiss Federal Institute of Technology—EPFL, 1015 Lausanne, Switzerland

Received 10 February 1998, in final form 5 May 1998

Abstract

Ferroelectric, dielectric and piezoelectric properties of ferroelectric thin films and ceramics are reviewed with the aim of providing an insight into different processes which may affect the behaviour of ferroelectric devices, such as ferroelectric memories and micro-electro-mechanical systems. Taking into consideration recent advances in this field, topics such as polarization switching, polarization fatigue, effects of defects, depletion layers, and depolarization fields on hysteresis loop behaviour, and contributions of domain-wall displacement to dielectric and piezoelectric properties are discussed. An introduction into dielectric, pyroelectric, piezoelectric and elastic properties of ferroelectric materials, symmetry considerations, coupling of electro-mechanical and thermal properties, and definitions of relevant ferroelectric phenomena are provided.

0034-4885/98/091267+58$59.50

Contents

1. Introduction

Interest in ferroelectric properties, materials and devices has been considerable over the last 10 years. On one hand, this interest has been driven by the exciting possibility of using ferroelectric thin films for nonvolatile memory applications and new microelectromechanical systems (MEMS). On the other hand, problems associated with applications of ferroelectric materials, such as polarization fatigue, ageing and field and frequency dependence of the piezoelectric, elastic and dielectric properties, generated intensive research of the fundamental properties of ferroelectrics. For most, if not for all currently considered applications, the main interest is in polycrystalline (ceramic) ferroelectrics and thin films, which are easier to make and which offer a larger variety of easily achievable compositional modifications than single crystals. The disadvantage of polycrystalline ferroelectrics and films is that their properties are often controlled by contributions from domain-wall displacements and other so-called extrinsic contributions, which are responsible for most of the frequency and field dependence of the properties, and whose theoretical treatment presents a considerable challenge. In addition, geometry of thin films imposes boundary conditions which sometimes lead to very different properties of films with respect to bulk materials and which must be taken into account when modelling devices.

This paper focuses on ferroelectric, dielectric and piezoelectric properties of ferroelectric thin films and ceramics and reviews recent advances in this field. The pyroelectric properties are discussed only in terms of effects of external fields on the pyroelectric response and coupling with the piezoelectric and elastic effects. In the first part dielectric, elastic, piezoelectric, electrostrictive and pyroelectric relationships are given in the tensor form and discussed in terms of the material symmetry. Coupling of temperature, elastic, dielectric, piezoelectric and pyroelectric variables is then introduced using the thermodynamic approach. This introductory discussion on the symmetry effects and variable coupling is thought to be important, especially for nonspecialists in the field who work with thin films. Films can be grown in many orientations and with different boundary conditions, both of which define film properties, so that understanding of symmetry effects and constraints imposed by variable coupling becomes essential. In the second part, the most important phenomena of ferroelectric materials (polarization, hysteresis, domain walls, phase transitions) are first introduced by giving basic definitions and using the thermodynamic Landau–Ginzburg–Devonshire (LGD) approach. The LGD approach is presented in some detail as it is the most powerful method to study the behaviour of ferroelectric materials and, in particular, effects of external fields on the properties. Results of LGD theory are used throughout the review. The ferroelectric (polarization reversal, hysteresis behaviour, polarization fatigue, ageing), dielectric and piezoelectric properties of ferroelectric ceramics and thin films are then discussed in more detail with the emphasis on the influence of domain-wall structure, domain-wall displacement, defects, microstructure, depletion and depolarization effects, and external electric and mechanical fields on the properties.

2. Symmetry of materials and tensor properties

2.1. Introduction

In this section the tensor definition of basic dielectric, elastic, piezoelectric, pyroelectric, and electrostrictive relationships is introduced. It is assumed that the reader is familiar with basic properties of tensors (see, for example, [1]). Coupling of elastic and electrical variables and temperature is introduced through the thermodynamic approach, again assuming a basic knowledge of thermodynamics. In all tensor relationships summation over repeated indices is assumed. Tensor indices are defined with respect to an orthogonal coordinate system, so that, for example, P_3 represents the component of electric polarization along the z-direction of an (x, y, z) orthogonal coordinate system. Axes of the coordinate system are oriented either along crystalographic axes of a crystal, or with the z-axis along the polarization direction of ceramics or, in the case of thin films, with the z-axis perpendicular to the plane of the film.

2.2. Tensor definition of the dielectric, piezoelectric, elastic, pyroelectric and electrostrictive coefficients

2.2.1. Dielectric permittivity. The polarization P_i (C m^{-2}) that is induced in an insulating, polarizable material (a dielectric) by an applied electric field vector E_i (V m^{-1}) is given by:

$$P_i = \chi_{ij} E_j \tag{1}$$

where χ_{ij} (F m^{-1}) is the second-rank tensor known as the dielectric susceptibility of the material. Relation (1) is valid only for linear materials or in a linear limit for nonlinear materials and, in general, P_i depends on higher-order terms of the field (see section 4.7). The total surface charge density that is induced in the material by the applied field is given by the dielectric displacement vector, D_i (C m^{-2}):

$$D_i = \varepsilon_0 E_i + P_i. \tag{2}$$

Scalar $\varepsilon_0 = 8.854 \times 10^{-12}$ F m^{-1} is known as the dielectric permittivity of a vacuum. It follows from (1) and (2) that

$$D_i = \varepsilon_0 E_i + \chi_{ij} E_j = \varepsilon_0 \delta_{ij} E_j + \chi_{ij} E_j = (\varepsilon_0 \delta_{ij} + \chi_{ij}) E_j = \varepsilon_{ij} E_j \tag{3}$$

where $\varepsilon_{ij} = \varepsilon_0 \delta_{ij} + \chi_{ij}$ is the dielectric permittivity of the material and δ_{ij} is Kronecker's symbol ($\delta_{ij} = 1$ for $i = j$, $\delta_{ij} = 0$, for $i \neq j$). For most ferroelectric materials $\varepsilon_0 \delta_{ij} \ll \chi_{ij}$ and $\varepsilon_{ij} \approx \chi_{ij}$. In practice, the relative dielectric permittivity, $\kappa_{ij} = \varepsilon_{ij}/\varepsilon_0$, also known as the dielectric constant of the material, is more often used than the dielectric permittivity.

Using free energy arguments it can easily be shown that χ_{ij} (as well as ε_{ij} and κ_{ij}) must be symmetrical tensor ($\chi_{ij} = \chi_{ji}$) with only six independent components [1–3]. Symmetry of a material may further reduce the number of independent components of the permittivity tensor (section 2.4).

2.2.2. Elastic compliance and stiffness. The relationship between the stress X_{ij} (N m^{-2}) applied upon an elastic material and resulting strain $x_{ij}(-)$ is given, in the linear approximation, by Hooke's law:

$$x_{ij} = s_{ijkl} X_{kl}. \tag{4}$$

The elastic compliance s_{ijkl} (m^2 N^{-1}) is a fourth-rank tensor and x_{ij} and X_{ij} are second-rank tensors. The inverse relationship $X_{ij} = c_{ijkl}x_{kl}$ defines elastic stiffness tensor c_{ijkl} (N m^{-2}). The relationship between s_{ijkl} and c_{ijkl} is given by $s_{ijkl}c_{klmn} = c_{ijkl}s_{klmm} = \delta_{im}\delta_{jn}$.

The strain and stress are by definition symmetrical second-rank tensors, i.e. $x_{ij} = x_{ji}$ and $X_{ij} = X_{ji}$. The symmetry of the strain and stress tensors requires that $s_{ijkl} = s_{jilk}$ so that the number of independent elements of the compliance and stiffness tensors is reduced from 81 to 36. Using thermodynamics it can be further shown that s_{ijkl} is a symmetrical tensor ($s_{ijkl} = s_{klij}$) and the number of independent elements is therefore reduced to 21 [1–3]. Further reduction of independent components is possible using material symmetry (section 2.4).

2.2.3. Piezoelectric effect. Piezoelectric materials are a class of materials which can be polarized, in addition to an electric field, also by application of a mechanical stress. The linear relationship between stress X_{ik} applied to a piezoelectric material and resulting charge density D_i is known as the *direct* piezoelectric effect and may be written as

$$D_i = d_{ijk}X_{jk} \tag{5}$$

where d_{ijk} (C N^{-1}) is a third-rank tensor of piezoelectric coefficients.

The piezoelectric materials have another interesting property, in that they change their dimensions (they contract or expand) when an electric field E is applied to them. The *converse* piezoelectric effect describes the strain that is developed in a piezoelectric material due to the applied electric field:

$$x_{ij} = d_{kij}E_k = d^t_{ijk}E_k \tag{6}$$

where t denotes the transposed matrix. The units of the converse piezoelectric coefficient are (m V^{-1}). The piezoelectric coefficients d for the direct and converse piezoelectric effects are thermodynamically identical (section 3.1) i.e. $d_{\text{direct}} = d_{\text{converse}}$. Note that the sign of the piezoelectric charge D_i and strain x_{ij} depends on the direction of the mechanical and electric fields, respectively. The piezoelectric coefficient d can be either positive or negative. It is common to call a piezoelectric coefficient measured in the direction of applied field the longitudinal coefficient, and that measured in the direction perpendicular to the field the transverse coefficient. Other piezoelectric coefficients are known as shear coefficients.

Because the strain and stress are symmetrical tensors, the piezoelectric coefficient tensor is symmetrical with respect to the same indices, $d_{ijk} = d_{ikj}$. The number of independent piezoelectric coefficients is thus reduced from 27 to 18. The number of independent elements of d_{ijk} may be further reduced by the symmetry of the material (section 2.4). As discussed in section 2.4 piezoelectric coefficients must be zero and the piezoelectric effect is absent in all 11 centrosymmetric point groups and in point group 432. Materials that belong to other symmetries may exhibit the piezoelectric effect.

Examples of piezoelectric materials are quartz (SiO_2), zinc oxide (ZnO), polyvinylidene fluoride (PVDF or $(CH_2CF_2)_n$)) and lead zirconate titanate, (PZT or $Pb(Zr, Ti)O_3$). The direct piezoelectric effect is the basis for force, pressure, vibration and acceleration sensors and the converse effect for actuator and displacement devices.

2.2.4. Pyroelectric and ferroelectric materials. Some materials, called polar or pyroelectric, exhibit electric dipole moment even in the absence of an external electric field. The polarization associated with a spontaneously formed dipole moment is called spontaneous polarization, P_S. The charge due to the spontaneous polarization is usually masked by charges from the surrounding of the material and it is experimentally easier to

observe changes in the spontaneous polarization. The change of the vector of spontaneous polarization with temperature T defines the pyroelectric effect:

$$p_i = \frac{\partial P_{S,i}}{\partial T} \tag{7}$$

where p_i (C m^{-2} K^{-1}) is the vector of pyroelectric coefficients. Equation (7) may be written in the form

$$D_i = \Delta P_{S,i} = p_i \Delta T \tag{8}$$

where D_i is the surface charge density induced in the material by the temperature change ΔT.

The spontaneous polarization can occur only in materials which possess a unique polar axis (section 2.4, [1]). These materials belong to 10 polar crystallographic point groups, which are a subset of noncentrosymmetric point groups. Thus, all pyroelectric materials are piezoelectric, but only some piezoelectric materials (those whose symmetry belongs to polar groups) are pyroelectric. Some examples of polar materials are ZnO, $(CH_2CF_2)_n$ and Pb(Zr, Ti)O_3. Note that pyroelectric materials only partially overlap with piezoelectric material listed in the above section.

Ferroelectric crystals are polar crystals in which direction of the spontaneous polarization can be switched by an external electric field. A more detailed definition of ferroelectric materials will be given in section 4. Thus, all ferroelectric materials are pyroelectric but only some pyroelectric materials (those in which polarization may be switched by external field) are ferroelectric. Clearly, all ferroelectric materials are piezoelectric.

2.2.5. Electrostrictive effect. The electrostrictive effect is an example of nonlinear coupling between elastic and electrical fields. If an electric field E_i is applied on a material, the electrostrictive strain x is defined by

$$x_{ij} = M_{ijkl} E_k E_l \tag{9}$$

where M_{ijkl} are components of the fourth-rank tensor and are called electrostrictive coefficients. Alternatively, the electrostrictive effect can be expressed in terms of the vector of induced polarization. Combining equations (1) and (9) one obtains

$$x_{ij} = Q_{ijkl} P_k P_l \tag{10}$$

where Q_{ijkl} and M_{ijkl} are related by

$$M_{ijmn} = \chi_{km} \chi_{ln} Q_{ijkl}. \tag{11}$$

The electrostrictive effect is present in all material, regardless of the symmetry. Formulation of the 'converse' electrostrictive effects is also possible [4].

In ferroelectric materials the polarization at strong fields is a nonlinear function of the electric field so that (9) and (10) cannot both be valid. Experimental results in, for example, $Pb(Mg_{1/3}Nb_{2/3})O_3$–$PbTiO_3$ solid solution show that (9) holds only at weak fields whereas (10) is always valid for the pure electrostrictive effect. This suggests that (10) is a more consistent way to describe the electrostrictive effect in dielectrically nonlinear materials. In section 4.7 we shall see that the piezoelectric effect in ferroelectrics may be interpreted as the electrostriction biased by the spontaneous polarization.

Assume now that a strong DC electric field and a weak AC electric field are applied simultaneously on a nonpiezoelectric material. For simplicity we omit tensor indices and write (9) as

$$x = M(E_{DC} + E_{AC})^2 = M E_{DC}^2 + 2M E_{DC} E_{AC} + E_{AC}^2. \tag{12}$$

Table 1. Rules for matrix notation [1, 6].

Tensor notation	Corresponding matrix notation
$ii = 11, 22, 33$	$m = 1, 2, 3$
$ij = 23$ or 32, 13 or 31, 12 or 21	$m = 4, 5, 6$
s_{ijkl}	s_{mn}, both m and $n = 1, 2, 3$
$2s_{ijkl}$	s_{mn}, m or $n = 4, 5, 6$
$4s_{ijkl}$	s_{mn}, both m and $n = 4, 5, 6$
d_{ijk}	d_{im}, $m = 1, 2, 3$
d_{ijk}	$\frac{1}{2}d_{im}$, $m = 4, 5, 6$
Q_{ijkl}	Q_{mn}, $m = 1, \ldots, 6$, $n = 1, 2, 3$
$2Q_{ijkl}$	Q_{mn}, $m = 1, 2, \ldots, 6$, $n = 4, 5, 6$

The term $(2ME_{\mathrm{DC}})E_{\mathrm{AC}}$ behaves like the piezoelectric effect (6), i.e. the strain is linear with respect to the AC field and changes sign when the AC field changes its direction. Since all materials show an electrostrictive effect, it follows that any material biased by a DC electric field will exhibit a piezoelectric effect under an external AC electric field. From the symmetry point of view it is not difficult to see that the combination 'material + DC electric field' is noncentrosymmetric. In most materials this induced piezoelectric effect is very small. Exception are so-called relaxor-ferroelectrics, such as $Pb(Mg_{1/3}Nb_{2/3})O_3$, where an electric-field-induced piezoelectric effect may be very large [5].

2.3. Matrix notation

To simplify notation, the elastic compliance and piezoelectric coefficient tensors may be written in the matrix or reduced notation form, following the Voigt convention given in table 1, [1]. A pair of indices $ii = 11, 22, 33$ is, for example, replaced with the single index $m = 1, 2, 3$, respectively, and the mixed pairs of indices (which represent shear components of strain and stress tensors) $ij = 23$ or 32, 13 or 31, 12 or 21 are written as $m = 4, 5, 6$, respectively.

Equations (4)–(6) can now be written in the following matrix format:

$$x_m = s_{mm}X_n \tag{13}$$

$$D_i = d_{im}X_m \tag{14}$$

$$x_m = d_{im}E_i \tag{15}$$

where $i = 1, 2, 3$ and $m, n = 1, 2, \ldots, 6$. It is important to emphasize that matrices for s, c, d, x, and X in the reduced notation do not transform as tensors when the coordinate system is changed.

The tensor of electrostrictive coefficients has 36 independent elements, some of which may be zero due to symmetry of the material [1]. Further reduction of the matrix elements due to energy arguments analogous to those indicate in section 2.2 for dielectric permittivity and elastic compliances is not possible for the electrostrictive effect.

2.4. Symmetry of materials

Symmetry of the material, whether it is a crystal, a thin film, a polycrystalline or an amorphous material, affects its properties. According to Neumann's principle, symmetry elements of all physical properties of material must include all symmetry elements of the

point group of the material. In other words, if a physical property is subjected to a symmetry element of the material, this property should not change its value [1].

It follows from the Neumann's principle that some properties (such as dielectric permittivity, elastic compliance and electrostriction) are present in all materials and that other properties (such as piezoelectricity and pyroelectricity) can exist only in materials with certain symmetries. Moreover, the symmetry requirements may significantly reduce the number of nonzero and independent elements of a property tensor. These arguments are usually demonstrated on examples of 32 crystal point groups. The piezoelectric and other effects described by odd-rank tensors are forbidden by the symmetry in crystals that belong to 11 centrosymmetric groups and in noncentrosymmetric point group 432. Crystals that belong to the remaining 20 noncentrosymmetric groups can exhibit the piezoelectric effect. These 20 point groups are sometimes called piezoelectric point groups. 10 of the piezoelectric point groups possess a unique polar axis and may exhibit, in the absence of an external electric field, a spontaneous polarization vector, P_S, and the pyroelectric effect along this unique axis. These 10 polar point groups are: 1, 2, m, $2mm$, 4, $4mm$, 3, $3m$, 6, and $6mm$. All ferroelectric crystals belong to one of these 10 polar point groups.

Crystallographic point groups with discrete symmetry elements are insufficient to describe polycrystalline and noncrystalline materials. Properties of a ceramic with random orientation of crystallites (or grains) are, for example, identical in all directions and may be described by introducing the symmetry axis of an infinite order [6], whose symbol is ∞. A symmetry axis of order ∞ means that material may be rotated by any angle around such an axis without changing its properties. The rotation axis of an isotropic cylinder, for example, is a ∞ axis. The point groups which contain infinity symmetry axes are called the limit groups of symmetry or Curie groups. There are seven Curie groups and all 32 crystallographic point groups are subsets of the Curie groups. Ceramic materials with a random orientation of grains possess spherical symmetry, $\infty\infty m$, which is centrosymmetric, and cannot exhibit a piezoelectric effect even if the symmetry of each grain belongs to one of the piezoelectric or polar point groups. If the ceramic is, however, ferroelectric, the spontaneous polarization direction in each grain may be reoriented by an external electric field in the direction of the field (section 4.3). Such a poled or polarized ceramic possesses symmetry of a cone, ∞m, and exhibits both piezoelectric and pyroelectric effects. The matrices of the elastic compliance, dielectric susceptibility, piezoelectric, electrostrictive and pyroelectric coefficients of poled ferroelectric polycrystalline materials with randomly oriented grains have the same nonzero matrix elements as crystals that belong to point group $6mm$ and are given in the appendix.

It is interesting to compare the effects of grain orientation on the symmetry of thin films and ceramics of the same material. Polycrystalline thin films of ZnO, which is a polar but nonferroelectric material, will show a strong piezoelectric and pyroelectric response. This is possible because grains of ZnO films usually grow with the crystal polar axis perpendicular to the substrate surface, figure 1, and in most, if not in all, of the grains the polarization is oriented in the same direction [7]. The grains are randomly distributed in the plane of the film that thus exhibits conical symmetry ∞m and piezoelectric and pyroelectric effects. Zinc oxide ceramics with randomly distributed grains possess spherical symmetry $\infty\infty m$ and do not exhibit the piezoelectric or pyroelectric effect. Those ceramics cannot become piezoelectric and pyroelectric by poling with an electric field because ZnO is a nonferroelectric material and the vectors of the spontaneous polarization cannot be oriented by an external electric field.

Symmetry considerations in ferroelectric thin films are more complex. Ferroelectric polycrystalline films may be grown with either preferential or random orientation of the

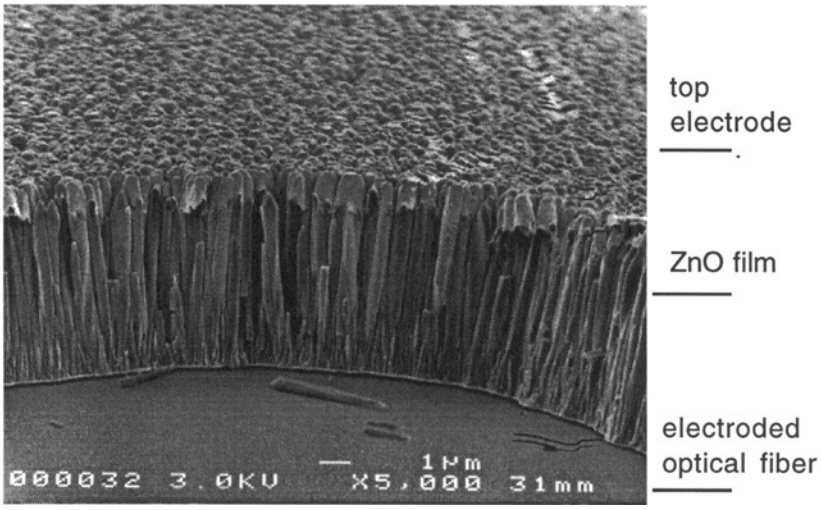

Figure 1. (002)-oriented ZnO thin film with columnar grains sputter deposited on an optical fibre. If the curvature of the fibre (radius of the fibre $\gg$ thickness of the film) is neglected, this section of the film possesses conical symmetry (∞m) and a large piezoelectric response. (Courtesy of G R Fox.)

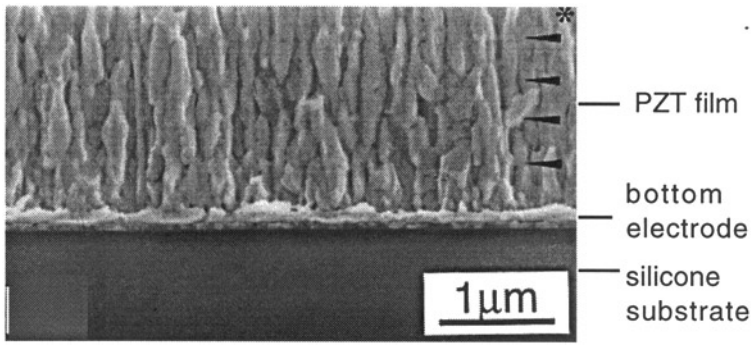

Figure 2. (111)-oriented $Pb(Zr_{0.45}Ti_{0.55})O_3$ sol-gel thin film deposited on a silicon wafer. Orientation of the film in the plane of the film is random. As-grown films usually exhibit nonzero polarization and conical symmetry (∞m). After thermal annealing polarization may drop to nearly zero and the symmetry of the film becomes cylindrical (∞/mm). (Courtesy of D V Taylor.)

grains. As-grown ferroelectric films which possess preferential orientation of grains along the z-axis (perpendicular to the plane of the film) and random orientation in the x–y plane (plane of the film) often exhibit nonzero polarization [8, 9] and therefore conical symmetry ∞m. This is, however, not always the case and averaging effects of ferroelectric domains (see sections 4.2 and 4.3) may lead to a very small or zero polarization even in such oriented films. Grain-oriented ferroelectric films with zero built-in polarization have nonpolar cylindrical symmetry $\frac{\infty}{m}m$ (figure 2), but can be polarized by an electric field to exhibit piezoelectric and pyroelectric properties. Likewise, ferroelectric films and ceramics with random grain orientation can be polarized by an electric field.

3. Coupling of thermal, electrical and mechanical properties

3.1. Thermodynamic relations

Electric charge in a polar material may be induced by an external electric field, equation (1), by a stress through the piezoelectric effect, equation (5), and by a temperature change through the pyroelectric effect, equation (8). Similarly, the mechanical strain in a piezoelectric material may be induced by an electric field through the converse piezoelectric effect, (6), by an external stress through Hooke's law, (4), and by a temperature change, due to the thermal expansion of the material. This coupling of different effects places important experimental constraints on property measurements. Assume, for example, that an electric field is applied on a piezoelectric material under constant temperature conditions. If the sample is mechanically free to change its dimensions, the resulting strain is due to the pure piezoelectric effect, equation (6). If the sample is partially clamped (for example a thin film deposited on a thick substrate), the resulting strain will be a sum of the piezoelectric strain, (6), and the mechanical strain, (4), defined by clamping conditions (see section 6.4.5).

The coupling between the thermal, elastic and electrical parameters of a material can be introduced formally using the thermodynamic approach. The results are equations of state which give relations between material parameters measured under different experimental conditions. These relations are essential for modelling and understanding the response of piezoelectric and pyroelectric devices. The approach is outlined below and a more detailed discussion can be found in [2, 3, 10].

It is well known from the first and second laws of thermodynamics that the reversible change $\mathrm{d}U$ in the internal energy U of an elastic dielectric that is subjected to a small change of the strain $\mathrm{d}x$, electric displacement $\mathrm{d}D$, and entropy $\mathrm{d}S$ is given by

$$\mathrm{d}U = T\,\mathrm{d}S + X_{ij}\,\mathrm{d}x_{ij} + E_i\,\mathrm{d}D_i \tag{16}$$

where T is the temperature of the material. Since in most experimental situations we work under isothermal conditions, and use electric field and stress as independent variables, it is useful to change the set of independent variables from (S, x, D) to (T, X, E). To change the independent variables from the original set to the other we perform a Legendre transformation of U by adding the expression $-Ts - Xx - ED$ to U. The resulting free energy function

$$G = U - TS - X_{ij}x_{ij} - E_i D_i \tag{17}$$

is known as the Gibbs free energy. The differential of G gives together with (16)

$$\mathrm{d}G = -S\mathrm{d}T - x_{ij}\,\mathrm{d}X_{ij} - D_i\,\mathrm{d}E_i. \tag{18}$$

From equation (18) one obtains

$$S = -\left(\frac{\partial G}{\partial T}\right)_{X,E} \qquad x_{ij} = -\left(\frac{\partial G}{\partial X_{ij}}\right)_{T,E} \qquad D_i = -\left(\frac{\partial G}{\partial E_i}\right)_{T,X} \tag{19}$$

where the subscripts indicate variables kept constant. The total differentials of S, X and D can be written as

$$\mathrm{d}S = \left(\frac{\partial S}{\partial T}\right)_{X,E}\mathrm{d}T + \left(\frac{\partial S}{\partial X_{ij}}\right)_{T,E}\mathrm{d}X_{ij} + \left(\frac{\partial S}{\partial E_i}\right)_{T,X}\mathrm{d}E_i \tag{20}$$

heat capacity; piezocaloric effect; electrocaloric effect

$$\mathrm{d}x_{ij} = \left(\frac{\partial x_{ij}}{\partial T}\right)_{X,E}\mathrm{d}T + \left(\frac{\partial x_{ij}}{\partial X_{kl}}\right)_{T,E}\mathrm{d}X_{ij} + \left(\frac{\partial x_{ij}}{\partial E_k}\right)_{T,X}\mathrm{d}E_k \tag{21}$$

thermal expansion; elastic compliance; converse piezoelectricity

$$\mathrm{d}D_i = \underbrace{\left(\frac{\partial D_i}{\partial T}\right)_{X,E}}_{\text{pyroelectric effect}} \mathrm{d}T + \underbrace{\left(\frac{\partial D_i}{\partial X_{jk}}\right)_{T,E}}_{\text{direct piezoelectricity}} \mathrm{d}X_{ij} + \underbrace{\left(\frac{\partial D_i}{\partial E_j}\right)_{T,X}}_{\text{dielectric permittivity.}} \mathrm{d}E_j \tag{22}$$

Each of the partial derivatives in equations (20)–(22) identifies a physical effect [1] as indicated in the equations. Since the order in which derivatives are taken is irrelevant [10] it follows from (18) and (20)–(22) that, for example

$$d_{ijk}^{T,X} = \underbrace{\left(\frac{\partial x_{ij}}{\partial E_k}\right)_{T,X}}_{\text{converse piezoelectric effect}} = -\left(\frac{\partial^2 G}{\partial E_k \partial X_{ij}}\right) = -\left(\frac{\partial^2 G}{\partial X_{ij} \partial E_k}\right) = \underbrace{\left(\frac{\partial D_k}{\partial X_{ij}}\right)_{T,E}}_{\text{direct piezoelectric effect}} = d_{kij}^{T,E} . \tag{23}$$

Equation (23) demonstrates the thermodynamic equivalence of the direct and converse piezoelectric effect. In a similar way it can be shown that the electrocaloric effect, $(\partial S/\partial E_i)_{T,X}$, is thermodynamically equivalent to the pyroelectric effect, $(\partial D_i/\partial T)_{X,E}$, and thermal expansion $(\partial x_{ij}/\partial T)_{X,E}$ to the piezocaloric effect $(\partial S/\partial X_{ij})_{T,E}$. Using other thermodynamic potentials which can be formed by taking Legendre transformations of the internal energy it is possible to write a total of 27 relationships such as (23) which are known as Maxwell relationships.

It is common to express equations (20)–(22) in the following integrated form, assuming that $\mathrm{d}E$ and $\mathrm{d}X$ represent small deviations from the zero initial stress and field [11]:

$$\Delta S = \frac{c^{X,E}}{T}\Delta T + \alpha_{ij}^{T,E} X_{ij} + p_i^{T,X} E_i \tag{24}$$

$$x_{ij} = \alpha_{ij}^{X,E}\Delta T + s_{ijkl}^{T,E} X_{kl} + d_{kij}^{T,X} E_k \tag{25}$$

$$D_i - p_i^{X,E}\Delta T + d_{ijk}^{T,E} X_{jk} + \varepsilon_{ij}^{T,X} E_j . \tag{26}$$

The superscripts in equations (24)–(26) denote variables held constant, α_{ij} is the thermal expansion tensor, and c is the heat capacity. Relations (20)–(22) and (24)–(26) include only linear effects. In the case of strong fields or strongly nonlinear material such as ferroelectrics, these relations must be extended to include higher-order terms. This will be done in section 4.7 on thermodynamics of ferroelectric materials.

3.2. Piezoelectric constitutive equations and electromechanical coupling factors

For isothermal processes, equations (25) and (26) written in matrix notation reduce to

$$x_m = s_{mn}^{T,E} X_n + d_{im}^{T,X} E_i \tag{27}$$

$$D_i = d_{im}^{T,E} X_m + \varepsilon_{ij}^{T,X} E_j . \tag{28}$$

Thus, the pure piezoelectric strain (charge) is obtained only under conditions of zero stress (zero electric field). Equations (27) and (28) are known as the piezoelectric constitutive equations.

The set of independent variables (T, E, X) chosen for the derivation of (24)–(26) was arbitrary. Other thermodynamic potentials and combinations of independent variables give six remaining isothermal piezoelectric constitutive equations:

$$X_m = c_{mn}^{E} x_n - e_{im}^{x} E_i \tag{29}$$

$$D_i = e_{im}^{E} x_m + \varepsilon_{ij}^{x} E_j \tag{30}$$

$$X_m = c_{mn}^{D} x_n - h_{im}^{x} D_i \tag{31}$$

$$E_i = -h_{im}^{D} x_m + \beta_{ij}^{x} D_j \tag{32}$$

$$x_m = s^D_{mn} X_n + g^X_{im} D_i \tag{33}$$

$$E_i = -g^D_{im} X_m + \beta^x_{ij} D_j \tag{34}$$

where $i, j = 1, 2, 3$, and $m, n = 1, 2, \ldots, 6$. e, g, and h are piezoelectric tensors and β is the inverse dielectric susceptibility ($=\chi^{-1}$). One important result of the thermodynamics of piezoelectric materials is that piezoelectric coefficients of the same type are thermodynamically equivalent: $d^X = d^E$, $g^D = g^X$, $e^x = e^E$, and $h^D = h^x$ and the superscripts are usually omitted.

Consider, as an illustration, the difference between g and d coefficients, while omitting matrix indices for simplicity. Relation $D = \mathrm{d}X$ gives piezoelectric charge measured on shorted samples, with free flow of the charge into the external electric circuit. If the sample is open circuited, this charge will accumulate on the sample surface and will generate electric field E across the sample. This field depends on capacitance (permittivity) of the sample (charge = capacitance × voltage) and is related to the stress by $E = -gX$ where $g = d/\varepsilon$. Which of relations (27)–(34) is to be used in a particular problem depends on the elastic and electric boundary conditions. The coefficients of piezoelectric tensors are mutually related by the following relationships:

$$d_{im} = e_{in} s^E_{nm} = \varepsilon^X_{ij} g_{jm} \qquad (\mathrm{m\ V^{-1}\ or\ C\ N^{-1}}) \tag{35}$$

$$e_{im} = d_{in} c^E_{nm} = \varepsilon^x_{ij} h_{jm} \qquad (\mathrm{C\ m^{-2}\ or\ V\ m\ N^{-1}}) \tag{36}$$

$$g_{im} = h_{in} s^D_{nm} = \beta^X_{ij} d_{jm} \qquad (\mathrm{m^2\ C^{-1}\ or\ N\ V^{-1}\ m^{-1}}) \tag{37}$$

$$h_{im} = g_{in} c^D_{nm} = \beta^x_{ij} e_{jm} \qquad (\mathrm{N\ C^{-1}\ or\ V\ m^{-1}}) \tag{38}$$

d is the charge or strain coefficient, e is the stress or charge coefficient, h is the stress or voltage coefficient, and g is the strain or voltage coefficient. Because of the piezoelectric coupling between electric and elastic fields, the values of the dielectric permittivity and elastic compliance (or stiffness) measured under different experimental conditions will not be the same. Take for example the dielectric permittivity measured on a clamped sample (conditions of constant (zero) strain). The tensory indices are omitted for simplicity. For $x = 0$, equation (29) together with (36) gives $X = -eE = -(d/s^E)E$. Inserting this stress into expression (28) for the dielectric displacement one obtains $D = (\varepsilon^X - d^2/s^E)E = \varepsilon^x E$ where

$$\varepsilon^x = \varepsilon^X (1 - d^2/s^E \varepsilon^X) = \varepsilon^X (1 - k^2) \tag{39}$$

is called the clamped (zero strain) dielectric constant. The combination $k^2 - d^2/s^E \varepsilon^X$ is known as the electromechanical coupling coefficient. In some ferroelectrics k may be as large as 0.7–0.9 [12] leading to as much as 50–80% difference between the free (zero stress) and clamped (zero strain) dielectric constant. It can be shown in a similar way that the elastic compliance s^D, measured under open-circuit conditions (zero or constant D), and compliance s^E measured under short-circuit conditions (zero or constant E), are related by

$$s^D = s^E (1 - d^2/s^E \varepsilon^X) = s^E (1 - k^2). \tag{40}$$

These two examples illustrate the importance of controlling experimental boundary conditions when measuring properties of piezoelectric materials. Similar experimental constraints exist for measurements of the pyroelectric coefficient (see section 7.2).

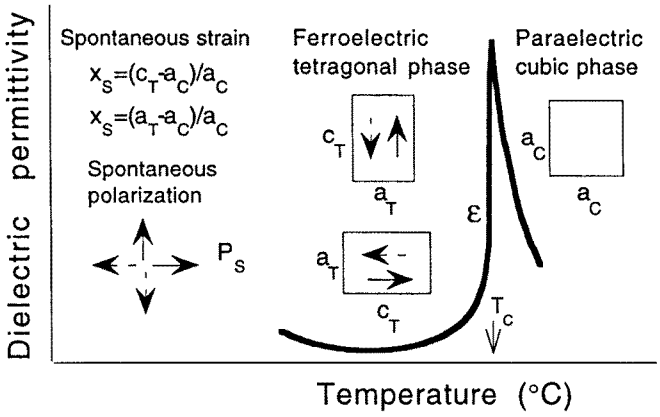

Figure 3. Illustration of the changes in a ferroelectric material which transforms from a paraelectric cubic into ferroelectric tetragonal phase with temperature. Such a phase transition is observed in $PbTiO_3$ and $BaTiO_3$. The permittivity curve represents data measured on a $BaTiO_3$ ceramic. The arrows show possible directions of the spontaneous polarization (in two dimensions). The unit cell is represented by a square in the cubic phase and rectangle in the tetragonal phase.

4. Ferroelectric properties

4.1. Definitions

Ferroelectrics are polar materials that possess at least two equilibrium orientations of the spontaneous polarization vector in the absence of an external electric field, and in which the spontaneous polarization vector may be switched between those orientations by an electric field. Readers interested in the theoretical treatment of ferroelectricity and related phenomena should consult classical textbooks on the subject [2, 3, 13]. Most ferroelectric materials undergo a structural phase transition from a high-temperature nonferroelectric (or paraelectric) phase into a low-temperature ferroelectric phase (figure 3). The paraelectric phase may be piezoelectric or nonpiezoelectric and is rarely polar [2]. The symmetry of the ferroelectric phase is always lower than the symmetry of the paraelectric phase. The temperature of the phase transition is called the Curie point, T_C. Above the Curie point the dielectric permittivity falls off with temperature according to the Curie–Weiss law

$$\varepsilon = \varepsilon_0 + \frac{C}{T - T_0} \approx \frac{C}{T - T_0} \tag{41}$$

where C is the Curie constant, T_0 ($T_0 \leqslant T_C$) is the Curie–Weiss temperature (see section 4.7). Some ferroelectrics, such as barium titanate, $BaTiO_3$, undergo several phase transitions into successive ferroelectric phases. Only transition temperature into the first ferroelectric phase is called the Curie point. The transition into a ferroelectric phase usually leads to strong anomalies in the dielectric, elastic, thermal and other properties of the material [2] and is accompanied with changes in the dimensions of the crystal unit cell. The associated strain is called the spontaneous strain, x_S. It represents the relative difference in the dimensions of the ferroelectric and paraelectric unit cells [14, 15]. The spontaneous strain is related to the spontaneous polarization via electrostrictive coefficients (section 4.7). Some changes that can occur in a ferroelectric material which transforms from a paraelectric cubic into a ferroelectric tetragonal phase are illustrated in figure 3.

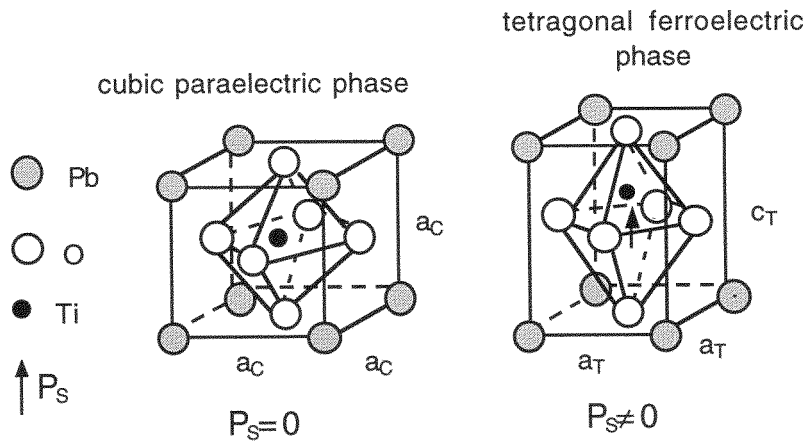

Figure 4. The perovskite structure ABO_3, shown here for $PbTiO_3$ which has a cubic structure in the paraelectric phase and tetragonal structure in the ferroelectric phase.

4.2. Ferroelectric domains

The spontaneous polarization in a ferroelectric crystal (or a grain in a ferroelectric film or ceramic) is usually not uniformly aligned throughout the whole crystal along the same direction. To avoid a too general discussion we take as an example lead titanate, $PbTiO_3$. Lead titanate is a perovskite crystal which transforms from a nonferroelectric cubic to a ferroelectric tetragonal phase at 490 °C. Perovskite crystals have the general formula ABO_3 where the valence of A cations is from $+1$ to $+3$ and of B cations from $+3$ to $+6$. As shown in figure 4, the structure may be viewed as consisting of BO_6 octahedra surrounded by A cations. Most of the ferroelectric materials that are of practical interest have perovskite structure and many form a solid solution with $PbTiO_3$. The spontaneous polarization in $PbTiO_3$ lies along the c_T-axis of the tetragonal unit cell and crystal distortion is usually described in terms of shifts of O and Ti ions relative to Pb ([16], section 4.8). In the ferroelectric phase the crystal is spontaneously strained with $a_T \leqslant a_C < c_T$ where a_T and a_C are the a-axes of the tetragonal and cubic unit cell.

The six directions (including positive and negative orientations) along the three a_C-axes of the cubic cell are equivalent, and the spontaneous polarization may arise with equal probability along any of them when the crystal is cooled through the ferroelectric phase transition temperature. The directions along which the polarization will develop depend on the electrical and mechanical boundary conditions imposed on the sample, as discussed below. The regions of the crystal with uniformly oriented spontaneous polarization are called ferroelectric domains. The region between two domains is called the domain wall (figure 5). The walls which separate domains with oppositely orientated polarization are called 180° walls and those which separate regions with mutually perpendicular polarization are called 90° walls (figure 5). Because the c_T and a_T axes in a tetragonal crystal are different, the angle between polarization directions on each side of a 90° domain wall is slightly smaller than 90° [17].

Ferroelectric domains form to minimize the electrostatic energy of depolarizing fields and the elastic energy associated with mechanical constraints to which the ferroelectric material is subjected as it is cooled through paraelectric–ferroelectric phase transition [2, 18–20]. Onset of the spontaneous polarization at the transition temperature leads to

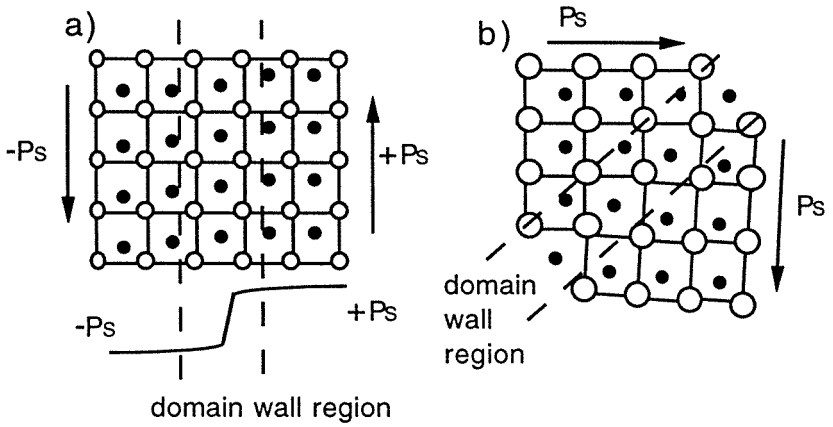

Figure 5. Illustration of (*a*) 180° and (*b*) 90° ferroelectric domains and domain-wall regions in a tetragonal perovskite ferroelectric. The schematic change of polarization across the domain wall is shown for a 180° wall in (*a*). Tetragonal distortion in (*b*) is exaggerated.

the formation of a surface charge. This surface charge produces an electric field, called a depolarizing field E_d, which is oriented oppositely to P_S (figure 6). The depolarizing field will form whenever there is a nonhomogeneous distribution of the spontaneous polarization, for example, due to the fall-off of the polarization near the surface of the ferroelectric (polarization is zero outside the ferroelectric and nonzero inside) or due to a change in the direction of polarization at grain boundaries. The depolarizing field may be very strong (on the order of MV m^{-1}) rendering the single-domain state of the ferroelectric energetically unfavourable [2, 18, 21]. The electrostatic energy associated with the depolarizing field may be minimized (i) if the ferroelectric splits into domains with oppositely oriented polarization (figure 6) or (ii) if the depolarizing charge is compensated for by electrical conduction through the crystal or by charges from the material surrounding (for example from the atmosphere or the electric circuit to which the material is connected). The depolarizing field often cannot be completely compensated for and as the grown ferroelectric crystals often exhibit reduced or even zero pyroelectric and piezoelectric effects due to the presence of ferroelectric domains.

Splitting of a ferroelectric crystal into domains may also occur due to an influence of mechanical stresses, as shown in figure 6 [20, p 98, 19]. Assume that a part of the $PbTiO_3$ crystal is mechanically compressed along the (100) cubic direction as it is cooled through the phase transition temperature. To minimize the elastic energy, the long c_T-axis of the tetragonal cell will develop perpendicularly to the stress. In the unstressed part of the crystal, polarization may remain parallel to the direction of the stress (short a_T-axis perpendicular to the stress). The domain walls in $PbTiO_3$ may therefore separate regions in which polarization orientation is antiparallel (180° walls) or perpendicular (90° walls) to each other. Both 90° and 180° walls may reduce the effects of depolarizing electric fields but only formation of 90° walls may minimize the elastic energy. A combination of electric and elastic boundary conditions to which a crystal is subjected as it is cooled through the ferroelectric phase transition temperature usually leads to a complex domain structure with many 90° and 180° walls.

Domain walls which differ in orientation to the spontaneous polarization vector are called ferroelectric domain walls and those which differ in orientation to the spontaneous strain

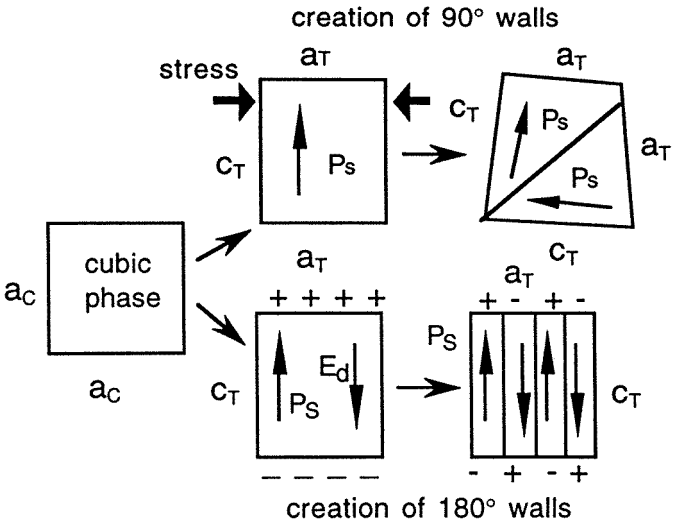

Figure 6. Formation of 90° and 180° ferroelectric domain walls in a tetragonal perovskite ferroelectric, such as $PbTiO_3$. The deformation of the crystal in the domain-wall region due to the formation of 90° walls is exaggerated for the sake of picture clarity. All symbols are explained in the text.

tensor are called ferroelastic domain walls. In $PbTiO_3$, 180° walls are purely ferroelectric because they differ only in the orientation of the polarization vector. 90° walls are both ferroelectric and ferroelastic as they differ both in orientation of the polarization vector and the spontaneous strain tensor.

The types of domain walls that can occur in a ferroelectric crystal depend on the symmetry of both the nonferroelectric and ferroelectric phases of the crystal [22]. In the rhombohedral phase of lead zirconate titanate, $Pb(Zr, Ti)O_3$, the direction of the polarization develops along the body diagonals (direction (111)) of the paraelectric cubic unit cell. This gives eight possible directions of the spontaneous polarization with 180°, 71° and 109° domain walls. Criteria which may be used to derive possible types of domain walls in a ferroelectric material were derived by Fousek and Janovec [22]. Ferroelectric domain walls are much narrower than domain walls in ferromagnetic materials. Observations with transition electron microscopy show that domain walls in ferroelectric thin films are on the order of 1–10 nm [2, 17].

4.3. Poling of ferroelectrics

Due to the complex set of elastic and electric boundary conditions at each grain, ferroelectric grains in ceramics and polycrystalline films are always split into many domains (figure 7). If the direction of the spontaneous polarization through the material is random or distributed in such a way as to lead to zero net polarization, the pyroelectric and piezoelectric effects of individual domains will cancel and such material is neither pyroelectric nor piezoelectric. Polycrystalline ferroelectric materials may be brought into a polar state by applying a strong electric field (10–100 kV cm^{-1}), usually at elevated temperatures. This process, called poling, cannot orient grains, but can reorient domains within individual grains in the direction of the field. A poled polycrystalline ferroelectric exhibits pyroelectric and piezoelectric properties, even if many domain walls are still present, figure 7. As-

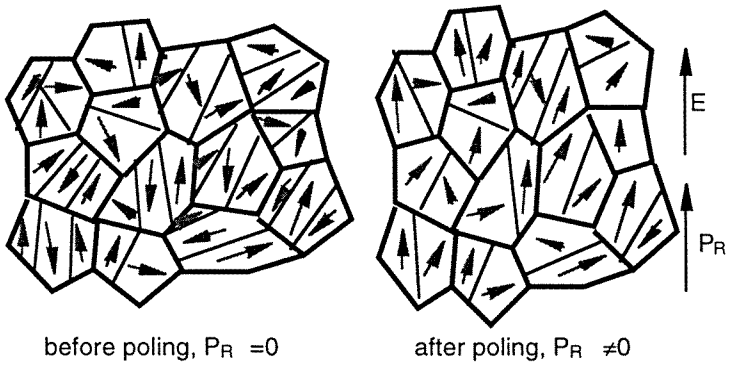

Figure 7. A polycrystalline ferroelectric with random orientation of grains before and after poling. Many domain walls are present in the poled material, however, the net remanent polarization is nonzero.

grown ferroelectric single crystals usually contain many domains and may exhibit weak piezoelectric and pyroelectric properties. A single crystal that does not contain domains is said to be in a single-domain or monodomain state. The single-domain state in single crystals may be achieved by poling.

Note again that, by definition (section 4.1), the poling, i.e. polarization reversal by a field, is possible only in ferroelectric materials. A pyroelectric (nonferroelectric) or piezoelectric polycrystalline material with randomly oriented grains cannot be poled and exhibit pyroelectric or piezoelectric properties.

The polarization after the removal of the field (at zero field) is called remanent polarization, P_R. Maximum remanent polarization that may be achieved in a polycrystalline material depends on available domain states. In a ferroelectric which exhibits only 180° domain walls the maximum remanent polarization $(P_R)_{\max}$ in the polycrystalline state is $0.25P_S$. In a tetragonal ferroelectric with six available domain states, $(P_R)_{\max} = 0.83P_S$. In a rhombohedral ferroelectric with eight possible domain states, $(P_R)_{\max} = 0.87P_S$. In an orthorhombic ferroelectric with 12 possible domain states, $(P_R)_{\max} = 0.91P_S$ [23, 24]. These values are ideal assuming reorientation of all domains along available directions dictated by the poling field. The actual polarization is in fact always lower, as many domains cannot be reoriented due to a complex set of internal stresses and electric fields in grains and because some domains will switch back after the poling field is removed. If the symmetry of the ferroelectric is such so as to allow non-180° domain walls, the poling process will change the sample dimensions, because reorientation of non-180° domains involves reorientation of the spontaneous strain (see figures 5 and 6).

4.4. Ferroelectric hysteresis loop and polarization switching

The most important characteristic of ferroelectric materials is polarization reversal (or switching) by an electric field. One consequence of the domain-wall switching in ferroelectric materials is the occurrence of the ferroelectric hysteresis loop (figure 8). The hysteresis loop can be observed experimentally by using a Sawyer–Tower circuit [25]. At small values of the AC electric field, the polarization increases linearly with the field amplitude, according to relation (1). This corresponds to segment AB in figure 8. In this region, the field is not strong enough to switch domains with the unfavourable direction of polarization. As the field is increased the polarization of domains with an unfavourable

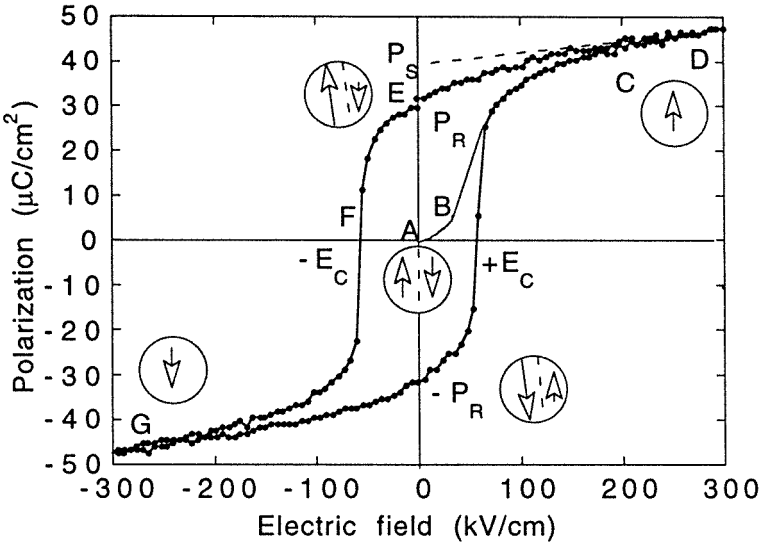

Figure 8. Ferroelectric (P–E) hysteresis loop. Circles with arrows represent the polarization state of the material at the indicated fields. The symbols are explained in the text. The actual loop is measured on a (111)-oriented 1.3 μm thick sol-gel $Pb(Zr_{0.45}Ti_{0.55})O_3$ film. (Experimental data courtesy of D V Taylor.)

direction of polarization will start to switch in the direction of the field, rapidly increasing the measured charge density (segment BC). The polarization response in this region is strongly nonlinear and equation (1) is no longer valid. Once all the domains are aligned (point C) the ferroelectricity again behaves linearly (segment CD). If the field strength starts to decrease, some domains will back-switch, but at zero field the polarization is nonzero (point E). To reach a zero polarization state the field must be reversed (point F). Further increase of the field in the negative direction will cause a new alignment of dipoles and saturation (point G). The field strength is then reduced to zero and reversed to complete the cycle. The value of polarization at zero field (point E) is called the remanent polarization, P_R. The field necessary to bring the polarization to zero is called the coercive field, E_C. The spontaneous polarization P_S is usually taken as the intercept of the polarization axis with the extrapolated linear segment CD. (Strictly speaking, in polycrystalline materials true spontaneous polarization equal to that of a single crystal can never be reached and it is more correct to speak of saturated rather than of spontaneous polarization.) It should be mentioned that the coercive field E_C that is determined from the intercept of the hysteresis loop with the field axis is not an absolute threshold field [18]. If a low electric field is applied over a (very) long time period the polarization will eventually switch.

An ideal hysteresis loop is symmetrical so that $+E_C = -E_C$ and $+P_R = -P_R$. The coercive field, spontaneous and remanent polarization and shape of the loop may be affected by many factors including the thickness of the film, the presence of charged defects, mechanical stresses, preparation conditions, and thermal treatment. Their effects on the hysteresis loop will be discussed in sections 5.2 and 5.3.

The mechanism of polarization switching has been studied in detail for many bulk and thin-film ferroelectrics [2, 18, 26]. The problem is clearly very complex and there does not seem to be a universal mechanism which would be valid for polarization reversal in all ferroelectrics. The polarization reversal takes place by the growth of existing antiparallel

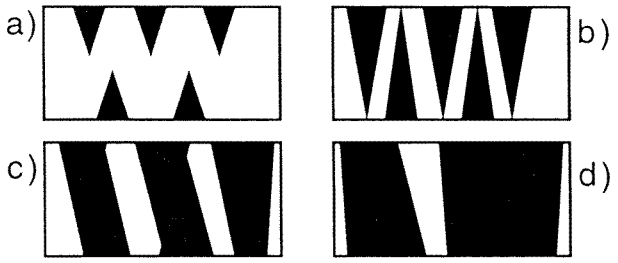

Figure 9. Probable sequence of polarization switching in ferroelectrics: (*a*) nucleation of oppositely oriented domains, (*b*) growth of oppositely oriented domains, (*c*) sidewise motion of domain walls and (*d*) coalescence of domains. Black and white areas have different orientation of polarization. (After Shur [21].)

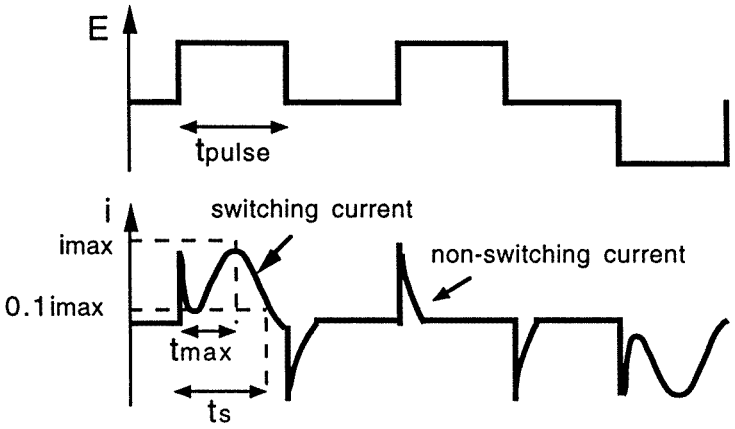

Figure 10. Switching and transient current during polarization switching. (*a*) Electrical field and (*b*) current as a function of time. (After Burfoot and Taylor [18].)

domains, by domain-wall motion, and by nucleation and growth of new antiparallel domains [2, 21, 27] (figure 9).

Experimentally, polarization switching is usually studied using pulsed (for example square-wave form) signal. This has two advantages. First, the field is constant during switching. Second, this arrangement is similar to that used for memory applications. Figure 10 shows a typical applied voltage wave form and switching current, $i \propto \mathrm{d}P/\mathrm{d}t$, for a ferroelectric. The field, applied antiparallel to the polarization, switches polarization from state $-P_R$ to $+P_R$. The total current consist of two parts. The first spike is due to the fast linear response of the dielectric and the bell-shaped curve is the current due to polarization switching. The total area under the curve is equal to

$$\int_0^{t_S} i(t)\,\mathrm{d}t = \varepsilon_0 \varepsilon E A + 2P_R A \tag{42}$$

where A is the area of electrodes. Once the ferroelectric is switched the same pulse may be applied again, this time parallel to polarization to obtain only the transient from the fast response of the dielectric. The area under the fast transient spike is $\varepsilon_0 \varepsilon E A$ and from this and equation (42) the remanent polarization may be calculated. The kinetics of polarization reversal may be described by measuring the switching time t_S for different amplitudes E of

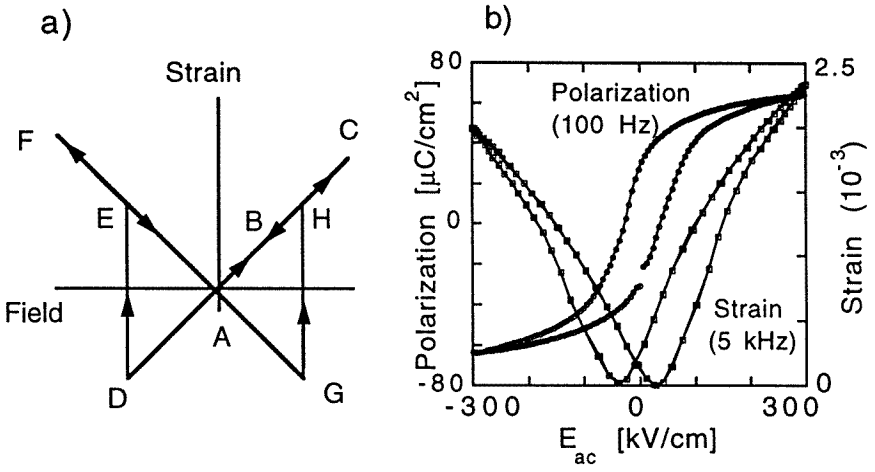

Figure 11. Strain–electric field (x–E) hysteresis loop (butterfly loop) in ferroelectrics: (*a*) idealized loop in a crystal in which polarization reverses only by 180° and (*b*) actual polarization and strain loops measured on (111)-oriented, 322 nm thick, sol-gel $Pb(Zr_{0.53}Ti_{0.47})O_3$ thin film. (Courtesy of D V Taylor.)

electric field pulse. Since the current decreases exponentially it is difficult to measure the total switching time, and t_S is usually taken as the value where current falls to $0.1i_{\max}$ [18]. The switching time can be expressed as

$$t_S = t_\infty e^{\alpha/E} \tag{43}$$

where α is the so-called activation field. At very high fields this relation changes to a power law of the form $t_S \propto E^{-n}$ where n depends on the material. The maximum switching current may be described by

$$i_{\max} = i_\infty e^{-\alpha/E}. \tag{44}$$

Constants α, n, t_∞ and i_∞ are temperature dependent, with switching time decreasing as the Curie point is approached. The switching times on the order of tens of nanoseconds were measured in Pb(Zr, Ti)O_3 ferroelectric thin films [28]. Care is needed when experimentally determining the switching time because the electrical time constant of the measuring circuit must be short compared with t_S [20].

It has recently been suggested that detailed information on nucleation, growth and coalescence of domains may be obtained from the switching current data [21]. The theoretical model of this approach is partly based on the classical Kolmogorov–Avrami theory of crystallization that was subsequently adapted to domain switching in ferroelectrics by Ishibashi and Takagi [29]. A description of the model and detailed discussion of polarization reversal may be found in a recent review paper by Shur [21].

4.5. Strain–electric field curve

In addition to the polarization–electric field hysteresis loop, polarization switching by an electric field in ferroelectric materials leads to strain–electric field hysteresis, as shown in figure 11. The strain–electric field hysteresis loop, which resembles the shape of a butterfly, is due to three types of effects. One is the normal converse piezoelectric effect of the lattice, and the other two are due to switching and movement of domain walls. Let us consider

as an example a monodomain single-crystal of $PbTiO_3$ and assume that polarization can be instantaneously switched by 180° reversal. To illustrate how the strain of the crystal changes during the field cycling we can use the following simple but instructive description [30].

At zero field (point A in figure 11(*a*)) the strain of the crystal is taken to be zero. The electric field is then applied in the direction of the spontaneous polarization. As the field is increased, the crystal expands through the piezoelectric effect, according to equation (6) and the strain traces the line A–B–C. The expansion continues until the maximum field is reached (point C). At point C the field starts to decrease, but is still parallel to P_S. The strain of the sample traces the same line but in the opposite direction (from C to A). At point A the strain is again zero. The field then changes its direction, becoming antiparallel to P_S. As the field strength increases in the negative direction, the crystal contracts with respect to point A, according to equation (6). At point D the field is large enough to switch the direction of polarization. After switching, the polarization becomes parallel to the field, and the strain becomes positive again (point E). During further increase of the field in the negative direction, strain increases to point F, and then decreases back to point A as the field is decreased in accordance with equation (6). The reversal of the polarization and sudden change of the strain happens again at point G. The strain–field curve is linear, indicating that the strain is purely piezoelectric except at the switching points D and G.

In reality, the strain–field relationship is more complicated, as shown in figure 11(*b*) for a (53/47)Pb(Zr, Ti)O_3 thin film (the ratio 53/47 describes the Zr/Ti ratio in the solid solution, see section 6.2). Ceramic samples usually contain a number of non-180° domains. The movement and switching of non-180° walls may involve a significant change in dimensions of the sample, in addition to the pure piezoelectric response of the material within each domain. The switching of the *a* and *c* axes of the tetragonal unit is, for example, accompanied by a strain of approximately 1% in $BaTiO_3$ ($a \sim 3.994$ Å, $c \sim 4.034$ Å at 20 °C, [31]) and 6% in $PbTiO_3$ ($a \sim 3.902$ Å, $c \sim 4.156$ Å at room temperature [16]). Clearly, there is no question of achieving such large strains in a ferroelectric material because only some parts of the sample contain non-180° walls, their orientation may be unfavourable and some of these walls will never switch under realizable experimental conditions. The contribution to the strain from the switching and movement of non-180° domain walls may, however, be comparable to the piezoelectrically induced strain. This has recently been shown experimentally by comparing total electric-field-induced strain and strain due to 90° domain-wall switching in a Pb(Zr, Ti)O_3-based ceramic [32]. The jump from one polarization orientation to another in real materials is less sudden than schematically shown in figure 11(*a*) because the coercive field may vary for different domains. During the field cycling a residual (or remanent) strain may be observed at zero field if domains in general do not switch to their original positions at zero field [33, 34]. The saturated, nonhysteretic, linear portion of the strain–field relationship may not even be observed in many experiments because the single-domain state may not be reached until very high fields. On the other hand, the contribution to the strain from movement of domain walls is strongly nonlinear and hysteretic, and it is this part of the strain–electric field relationship which is most often experimentally observed.

4.6. Domain-wall contribution to the properties of ferroelectric materials

In the previous sections we have seen how creation, propagation and switching of domains contributes to the ferroelectric polarization and strain hysteresis loops. Clearly any process that inhibits nucleation of new oppositely oriented domains or reduces the movement of

domain walls will affect the polarization and strain hysteresis loop characteristics. In addition to processes associated with polarization reversal, ferroelectric domain walls may move under weak and moderate (subswitching) fields, either by vibration or bending around an equilibrium position or by small jumps into a new equilibrium state. The displacement of domain walls at subswitching external fields has a profound influence on the dielectric, mechanical and piezoelectric properties of ferroelectric materials. Small displacements of all types of domain walls will affect the polarization of the material whereas the movement of non-180° walls will, in addition to the polarization change, directly contribute to the piezoelectric effect [23] (section 6.4.2). Movement of domain walls at weak to moderate fields is one of the most important so-called extrinsic (nonlattice) contributions to the dielectric, elastic and piezoelectric properties of ferroelectric materials [23, 35–38] and may be comparable to the intrinsic effect of the lattice [39, 40].

Real ferroelectrics, and especially ceramics and thin films nearly always contain electrical and elastic defects and imperfections that can interfere in a number of ways with domain walls and polarization within individual domains (sections 5.3.3 and 5.6). In most cases the defects inhibit domain-wall movement. It is said that domain walls become pinned or clamped by the defects and imperfections. Some common domain-wall pinning defects include oxygen vacancies and electrons trapped in the domain-wall area. An oxygen vacancy–acceptor dipole pair, on the other hand, may interact with polarization within a domain and make switching of the domain more difficult, effectively clamping the domain wall (see sections 5.6 [23, 41]). Displacement of domain walls also contributes to the dielectric and mechanical losses of ferroelectric materials and, particularly near the phase transition temperature, may dominate other loss mechanisms. The grain size, dopants, crystallographic orientation and crystal structure, external stresses, electric fields and preparation conditions of ceramics and thin films may through various processes affect domain-wall displacement. Effects of domain-wall movement on the properties of ferroelectric materials will be discussed in more detail in the following.

4.7. Thermodynamics of ferroelectrics

Transition into a ferroelectric state may be of the first or second order. The order of the phase transition is defined by the discontinuity in the partial derivatives of the Gibbs free energy of the ferroelectric at the phase transition temperature. For an nth-order phase transition, the nth-order derivative of G is a discontinuous function at the transition temperature [3]. Thus, spontaneous polarization and strain change continuously at the phase transition for a ferroelectric with the second-order phase transition, and are discontinuous at the phase transition temperature for first-order ferroelectrics (see (19), where $D = P_S$ in the absence of an external electric field). Barium titanate is an example of a ferroelectric with a first-order phase transition and lithium niobate, $LiNbO_3$ is a ferroelectric with a second-order phase transition. There is another type of ferroelectric-like materials, such as $Pb(Mg_{1/3}Nb_{2/3})O_3$, which are known as relaxor ferroelectrics or relaxors [23]. They are characterized by a chemical heterogeneity on nanometre scale. Relaxors display a diffuse phase transition with a broad maximum in the dielectric permittivity and a strong frequency dispersion of the permittivity below the temperature of the maximum permittivity (figure 12). Above the temperature of the maximum permittivity, relaxors do not obey the Curie–Weiss behaviour. The Curie temperature, the broadness of the permittivity peak and even the nature and the sequence of the phase transitions may be affected by preparing ferroelectrics in a thin-film form. Those effects will be discussed in the following.

Using thermodynamic functions it is possible to describe many important features of

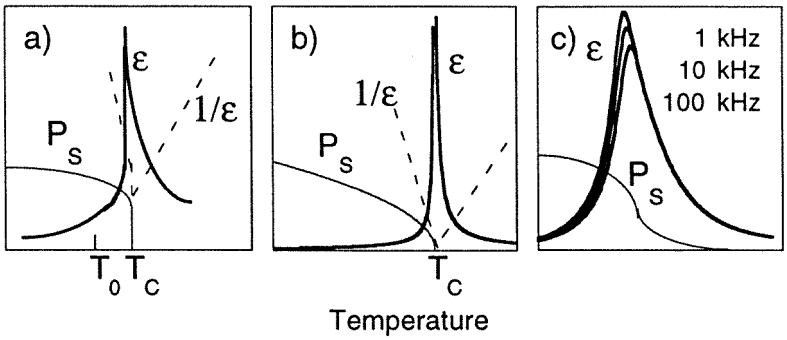

Figure 12. Schematic temperature dependence of the dielectric permittivity ε and spontaneous polarization P_S for (*a*) a first- and (*b*) a second-order ferroelectric and (*c*) for a relaxor ferroelectric. Permittivity data in (*c*) are measured on a $Pb(Mg_{1/3}Nb_{2/3})O_3$ ceramic. (Dielectric data courtesy of O Steiner.)

ferroelectric materials without going into microscopic mechanisms of ferroelectricity of the material under consideration. It follows from the basic thermodynamic relations that the stable phase under a given set of independent variables is the one which minimizes the corresponding free energy [3]. If we express the free energy as a function of independent variables, the condition of a minimum in the free energy will give possible stable phase(s) as well as expressions which relate dependent and independent variables. The usual approach is outlined in the following paragraphs [2, 3, 23]. Ferroelastic phase transitions can be treated in the same way. An excellent introduction into the thermodynamic treatment of nonferroelectric ferroelastic materials can be found in a recent book by Salje [42].

A set of variables appropriate for the particular problem is chosen. For ferroelectric phase transitions it is common to choose the (D (or P), X, T) set. Note that one can choose D or P as a variable, since $D = \varepsilon_0 E + P$ and $D = P_S$ in ferroelectric materials in the absence of an external electric field. Arguments for choosing D are discussed by Lines and Glass in their classical book [2, p 62]. The corresponding free energy function is called the elastic Gibbs energy G_1 which is obtained from the internal energy U by taking the following Legendre transformation: $G_1 = U - TS - X_i x_i$. By using equation (16) it is immediately seen that $\mathrm{d}G_1 = -S\,\mathrm{d}T - x_i\,\mathrm{d}X_i + E_i\,\mathrm{d}D_i$. The advantage of choosing the elastic Gibbs energy is that (i) it is possible to express the free energy in terms of the polarization (dielectric displacement) which is the order parameter of the phase transition. (The order parameter is the macroscopic parameter that appears in the less symmetric phase in a symmetry-breaking phase transition. In the case of the ferroelectric phase transitions, the order parameter is usually polarization [43].) (ii) It gives the relation between electric field and polarization under common experimental conditions of constant temperature and stress, i.e. $E_i = (\partial G_1/\partial D_i)_{X,T}$. (iii) G_1 is related to the Gibbs free energy G by $G = G_1 - E_i P_i$, i.e. $G_1 = G$ at $E = 0$. The minimum in the Gibbs free energy describes the stable phases under common experimental conditions of constant T, X and E. Once G_1 is known as a function of D (or P), G can be expressed as a function of displacement (polarization) under constant electric field E by $G = G_1 - E_i D_i$.

For small changes in D, X and T, the elastic Gibbs free energy can be expanded in a Taylor series around the equilibrium state $G_{10}(T)$ in which $D = 0, X = 0$, in terms of

independent variables, T, X and D as

$$G_1 = G_{10}(T) + \left(\frac{\partial G_1}{\partial T}\right)\Delta T + \left(\frac{\partial G_1}{\partial X_{ij}}\right)X_{ij} + \left(\frac{\partial G_1}{2D_i}\right)D_i + \frac{1}{2}\left(\frac{\partial^2 G_1}{\partial T^2}\right)\Delta T^2 + \frac{1}{2}\left(\frac{\partial^2 G_1}{\partial X_{ij}\partial X_{kl}}\right)X_{ij}X_{kl} + \frac{1}{2}\left(\frac{\partial^2 G_1}{\partial D_j \partial D_i}\right)D_i D_j + \left(\frac{\partial^2 G_1}{\partial T \partial X_{ij}}\right)\Delta T X_{ij} + \left(\frac{\partial^2 G_1}{\partial T \partial D_i}\right)\Delta T D_i + \left(\frac{\partial^2 G_1}{\partial X_{ij}\partial D_k}\right)X_{ij}D_k + a\Delta T^3 + b_{ijk}D_i D_j D_k + c_{ijklmn}X_{ij}X_{kl}X_{mn} + \text{higher-order terms} \quad (45)$$

where b_{ijk} and c_{ijklmn} are third-order derivatives of G_1 with respect to D and X. The free energy is usually measured from the paraelectric state which is assumed to be nonpolar. It is further assumed that the same analytical function describes both the paraelectric and ferroelectric phases [2, 44]. Coefficients in the Taylor expansion transform as products of the associated tensor components. For example, $b_{ij} = \frac{1}{2}(\partial G_1/\partial D_j \partial D_i)$ transforms as $D_i D_j$, i.e. as a second-order tensor and $g_{ijk} = (\partial G_1/\partial X_{ij}\partial D_k)$ transforms as a third-rank tensor. If the nonpolar phase is centrosymmetric, which is the case for most ferroelectrics of interest here, then it can be easily shown that all coefficients associated with odd-rank tensors must be zero (see section 2.4). This significantly reduces the number of terms which must be considered in equation (45). Furthermore, since the terms in the expansion represent correction terms, it is usually sufficient to terminate expansion with fourth or sixth-order terms. Assuming, for the purposes of illustration, the simplest one-dimensional case where polarization may occur only in one direction (+ and − orientation), and that the fields are applied parallel to polarization one obtains from (45) the following expression:

$$G_1 = G_{10}(T) + \tfrac{1}{2}\alpha_1 D^2 + \tfrac{1}{4}\alpha_2 D^4 + \tfrac{1}{6}\alpha_3 D^6 + \tfrac{1}{2}sX^2 + QXD^2 + \cdots. \quad (46)$$

Coefficients $\alpha_1, \alpha_2, \alpha_3, s$ and Q may be identified by using equation (45) (see also below). Usually only coefficient α_1 is assumed to be temperature dependent. A simple temperature dependence which will satisfy requirements for the minimum in the free energy above and below T_C ($G_1 = G_{10}$, $P = 0$ for $T > T_C$ and $G_1 < G_{10}$, $P \neq 0$ for $T < T_C$) and for continuity of the free energy at the transition temperatures is the linear temperature dependence in the form $\alpha_1 = (T - T_0)/C$ where C is a positive constant [10]. This choice of the temperature dependence of α_1 also gives the Curie–Weiss dependence of the permittivity above T_C, equation (41), which is in agreement with experimental observations in most ferroelectrics. α_3 must be positive because, for stability reasons, G_1 cannot become $-\infty$ as $D \to +\infty$. It can be shown that the order of the phase transition depends on the sign of α_2. The transition is of second order for $\alpha_2 > 0$ and of first order for $\alpha_2 < 0$. Using appropriate derivatives of G_1 and boundary conditions it is possible to calculate the temperature dependence of the spontaneous polarization, permittivity, pyroelectric and piezoelectric coefficients, as well as the effects of external fields (electric and elastic) on these properties and phase transition behaviour. Below we give three simple examples for a ferroelectric with a second-order phase transition as an illustration of this approach. Details may be found in [2, 3, 23].

A stable state of the system under conditions of fixed temperature, stress and electric field is obtained when the Gibbs free energy $G = G_1 - ED$ is minimal. The conditions for the minimum with $X = 0$ are

$$E = \left(\frac{\partial G_1}{\partial D}\right) = \alpha_1 D + \alpha_2 D^3 + \alpha_3 D^5 \quad (47)$$

and

$$\frac{1}{\varepsilon} = \left(\frac{\partial E}{\partial D}\right) = \left(\frac{\partial^2 G_1}{\partial D^2}\right) = \alpha_1 + 3\alpha_2 D^2 + 5\alpha_3 D^4 > 0. \tag{48}$$

If $E = 0$, then $D = P_S + \varepsilon E = P_S$ and equation (47) becomes

$$P_S(\alpha_1 + \alpha_2 P_S^2 + \alpha_3 P_S^4) = 0. \tag{49}$$

For $P_S = 0$, the materials is in the paraelectric phase. In the ferroelectric phase, for $P_S \neq 0$, equation (31) gives

$$P_S^2 = \frac{-\alpha_2 + (\alpha_2^2 - 4\alpha_1\alpha_3)^{1/2}}{2\alpha_3} \tag{50}$$

where only solutions with real values of polarization are chosen. For $\alpha_2^2 \gg \alpha_1\alpha_3$ the square root may be expanded in a series, and by keeping only the first-order term we obtain

$$P_S^2 = -\frac{\alpha_1}{\alpha_2} = -\frac{(T - T_0)}{\alpha_2 C} \qquad T < T_0, \alpha_2 > 0. \tag{51}$$

The same solution would have been obtained if the sixth-order term containing α_3 in (46) was neglected. A solution for P_S must satisfy the condition for the stability of the ferroelectric phase below $T_C (G_1 < G_{10}(T)$ and $P_S \neq 0)$ and the condition that $G_1 = G_{10}(T)$ above T_C. One can easily verify that this is indeed the case for the solution given in (51) if $T_0 = T_C$. Equation (51) gives two possible orientations of P_S ($+P_S$ and $-P_S$) as required by the definition of ferroelectricity. With this information for $P(T)$ it is now possible to calculate the temperature dependence of the permittivity. For $E = 0$, equation (48) gives

$$\frac{1}{\varepsilon} = \alpha_1 + 3\alpha_2 P_S^2 + 5\alpha_3 P_S^4. \tag{52}$$

In the paraelectric phase $P_S = 0$ and equation (52) becomes identical to the Curie–Weiss behaviour:

$$\frac{1}{\varepsilon} = \alpha_1 = \frac{T - T_0}{C} \qquad T > T_0 = T_C. \tag{53}$$

In the ferroelectric phase ($P_S \neq 0$) and in the vicinity of the transition temperature the term with the fourth power of polarization in (52) may be neglected because the spontaneous polarization is very small. It follows form (51) and (52) that the reciprocal permittivity below the phase transition has the following form:

$$\frac{1}{\varepsilon} = -2\alpha_1 = -2\left(\frac{T - T_0}{C}\right) \qquad T < T_0 = T_C. \tag{54}$$

The transition temperature T_C may be easily determined experimentally. To determine the Curie constant C and α_2 two additional experimental points for $P(T)$ and $\varepsilon(T)$ are required. Once these parameters are known, the temperature dependence of the polarization and the permittivity can be calculated.

The spontaneous strain x_S may be calculated from (46) by taking $X = 0$ and $E = 0$ (see equation (19)) as

$$x_S = \left(\frac{\partial G_1}{\partial X}\right) = Q P_S^2 \tag{55}$$

where Q is the electrostrictive coefficient. Note that spontaneous strain accompanies spontaneous polarization: if the system spontaneously polarizes, it will spontaneously strain through the electrostrictive effect. If the spontaneous strain is known as a function of the

temperature (for example from x-ray diffraction data) the electrostrictive coefficient may be calculated from (51) and (55).

The piezoelectric voltage coefficient $g = \left(\frac{\partial E}{\partial X}\right)$ (see equation (34)) may be obtained from (47) as

$$g = \left(\frac{\partial E}{\partial X}\right) = \left(\frac{\partial^2 G_1}{\partial X \partial D}\right) = 2QP_S. \tag{56}$$

By combining (56) and (35) one obtains

$$d = 2\varepsilon Q P_S. \tag{57}$$

The piezoelectric effect of ferroelectrics with centrosymmetric paraelectric phase may thus be considered as the electrostrictive effect biased by the spontaneous polarization. The temperature dependence of the piezoelectric constant can be calculated from equations (51), (54) and (57).

Similar relations may be derived for ferroelectrics with the first-order phase transition where now $\alpha_2 < 0$ and all terms in equation (50) are kept (sixth-order term in (46), which includes α_3, is no longer neglected). G_1 can now have equal minima at $P = 0$ and $P \neq 0$. Polarization and permittivity then become discontinuous functions of the temperature (figure 12) and the condition for stability of the ferroelectric phase requires that $T_C > T_0$ [2, 11].

Once all coefficients in the expansion of the thermodynamic potential are known it is, at least in principle, possible to calculate behaviour of the ferroelectric, including the temperature range where different phases of the ferroelectric are stable, and the dependence of the various material properties as a function of the temperature and external fields. Detailed calculations of the dielectric, piezoelectric and elastic coefficients have been made using the thermodynamic approach (often called LGD or Landau–Ginzburg–Devonshire theory) for many ferroelectric materials, including $BaTiO_3$ [45], $Pb(Zr, Ti)O_3$ solid solution [46], $Bi_4Ti_3O_{12}$ [47], and other ferroelectrics [3].

The derived thermodynamic relations are valid for a single-crystal ferroelectric in the monodomain state. To calculate values of the material coefficients for a polycrystalline ferroelectric, it is necessary to average single-crystal properties over all possible orientations of grains and domains within grains. Several methods for the averaging were reported in the literature [48–51]. In the case of the piezoelectric effect, equation (57) has been used for separation of extrinsic and intrinsic contributions to the piezoelectric response. The following procedure is used [36, 49]. It is assumed that relation of the same type as (57) is valid in polycrystalline ferroelectrics, where ε, Q and P_S are now averaged over all possible orientations of grains and domains. Those values can, in principle, be obtained from thermodynamic calculations and the averaging procedure. If a piezoelectric coefficient, for example, measured as a function of temperature, exhibits behaviour which differs from calculated, the difference between measured and calculated values is taken as the extrinsic contribution. The extrinsic contributions in ferroelectric materials are mostly due to the displacement of domain walls [35–37, 52], but other processes in a ferroelectric may also contribute to or even dominate the extrinsic component of the experimentally observed response [53]. Extrinsic contributions to the dielectric and piezoelectric properties of ferroelectric materials will be discussed in more details in sections 5.6, 6.4.3 and 6.4.4.

Extensions of the appropriate thermodynamic functions have been used to study effects of surface layers, depolarization effects [54, 55], space charges [56] and internal bias fields [57] on the phase transition behaviour and dielectric response of ferroelectrics. Effects of clamping stresses [58, 59] on the phase transitions and properties of thin films are discussed in more detail in section 5.4.1.

4.8. Microscopic theories and crystal structure considerations

Modern theory of ferroelectricity is based on lattice dynamics and the concept of so-called soft modes [2, 44, 60]. Ferroelectric phase transitions are a special case of structural phase transitions, and can thus be interpreted in terms of stability of the crystal-lattice dynamics. In a structural phase transition, the order parameter (polarization in the case of a ferroelectric phase transition (section 4.7)) may be associated with a lattice vibrational mode which exhibits an instability at the transition temperature. For a second-order transition, for example, the frequency spectrum of the lattice vibration related to the order parameter is proportional to $T - T_C$, so that this mode 'softens' (its frequency goes to zero) as the material is cooled toward T_C. Freezing of the vibrations at T_C gives rise to a nonzero-order parameter and the corresponding reduction in symmetry. A soft mode is an optic mode and can be studied experimentally by infrared spectroscopy and neutron scattering [44]. A detailed discussion of the theoretical approach can be found in the book by Lines and Glass [2].

The lattice dynamics approach and its recent extensions [61] have been very successful in describing qualitatively ferroelectric phase transitions. Difficulties in quantitative predictions originate in model simplifications which are often unavoidable in many-body problems. Whereas the phase transition sequence, effective charges of ions and polarization can now be fairly accurately calculated for many pure ferroelectrics, predictions of piezoelectric behaviour based on microscopic theories are still not available for any ferroelectric. Moreover, ferroelectricity in solid solutions, such as technologically the most important ferroelectric $Pb(Zr, Ti)O_3$, has been addressed for the first time only recently [62]. The picture of microscopic mechanisms that are responsible for the morphotropic phase behaviour in $Pb(Zr, Ti)O_3$ (see section 6.2) has not yet emerged, however, the preliminary calculations suggest that the simultaneous competition between phase separation of rhombohedral and tetragonal phases, long-range order and disorder of Zr and Ti may contribute to the extraordinary properties of this material.

From the structural point of view, the onset of polarization in simple perovskite ferroelectrics (see figure 4, section 4.2), such as $BaTiO_3$ and $PbTiO_3$ can be described by shifts of Ti and O ions relative to the large *A*-site cation. Both materials transform from a cubic paraelectric to a tetragonal ferroelectric phase ($T_C(BaTiO_3) = 120\,^\circ C$, $T_C(PbTiO_3) = 490\,^\circ C$). At the phase transition temperature, O and Ti ions in $BaTiO_3$ move in opposite directions, whereas in $PbTiO_3$ all ions move in the same direction relative to the position of *A* cation at the centre of the coordinate system. Ionic shifts are much larger in $PbTiO_3$ [2] leading to a larger spontaneous polarization ($P_S(PbTiO_3) = 57$–$75\ \mu C\ cm^{-2}$) and strain ($x_S \approx 6\%$) than in $BaTiO_3$ ($P_S(BaTiO_3) = 27\ \mu C\ cm^{-2}$, $x_S \approx 1\%$) at $20\,^\circ C$. The strongly covalent character of Pb–O bonding in $PbTiO_3$ probably plays an important role in ferroelectricity and large polarization of this material. Application of an external electric field in the direction of polarization will further displace ions, stretching the bonds. Thus, both the polarization and strain of these crystal will change, leading respectively to the dielectric and piezoelectric response.

Whereas simple crystallographic arguments may lead to an intuitive and qualitative understanding of electromechanical effects in simpler compounds, even this level of understanding is more difficult to achieve in more complex materials, as shown in the next example. The bismuth titanate-based family of layered-structure ferroelectrics is important because of large transition temperatures, fatigue-free polarization and stable piezoelectric properties in some compounds (sections 5.3 and 6.4). These materials belong to Aurivillius phases, and consist of alternating perovskite-like $A_{n-1}B_n O_{3n+1}$ and fluorite-like Bi_2O_3

layers, where A is a mono-, di- or trivalent cation, B is a cation with a valence of 4, 5 or 6, and n is the number of perovskite-like layers [63]. It appears that $Bi_4Ti_3O_{12}$ is one of the few compounds within the family that has a monoclinic ferroelectric structure, with one component of the polarization in the plane of the layers, and the other perpendicular to this plane. The resulting domain-wall structure is complex, leading to a considerable contribution to the piezoelectric properties (section 6.4.4). In many other compositions that belong to this family the ferroelectric phase seems to be orthorhombic with spontaneous polarization confined in the plane of the layers [64]. Many of these (pseudo-)orthorhombic compounds, such as $SrBi_4Ti_4O_{15}$ exhibit stable piezoelectric properties (section 6.4.4). Owing to a recent refinement [65] of the $Bi_4Ti_3O_{12}$ structure in the ferroelectric phase, it now seems that the origin of the large polarization within the plane of layers may be traced to a large displacement of Bi^{+3} cations in the perovskite A sites with respect to the chain of TiO_6 octahedra. The small polarization in the direction perpendicular to the plane of layers is related to a small displacement of the Ti cation. Calculations show that Bi^{+3} in the A site is strongly underbonded, and Ti^{+4} in the B site slightly overbonded. The need to satisfy bond valence requirements is identified as the driving force for the cation displacement. Partial replacement of Bi with divalent cations such as Sr may change bonding requirements and modify the driving force for the onset of polarization in different directions. As a result, domain-wall structure in modified compounds may be different and/or may respond to external fields in a different way than in monoclinic $Bi_4Ti_3O_{12}$. Whether the above crystallographic arguments may indeed explain the absence of domain-wall contributions to the piezoelectric properties in some of the bismuth titanate-based compounds remains, however, an open question as detailed structural data for those materials are presently not available. Crystallographic arguments and the role of chemical bonding in ferroelectric phase transitions have been discussed qualitatively for many ferroelectric compounds by Megaw [66].

5. Effects of defects, microstructure and external fields on the ferroelectric properties

5.1. Introduction

In real ferroelectrics the properties are strongly influenced by the microstructure, defects, compositional inhomogeneity, external fields, and domain-wall displacement. These external factors may not only contribute to the properties but in many cases may actually control the material response. In films, the thickness plays an additional role. Ferroelectricity is due to relatively 'long-range' interactions of dipoles and stability of the ferroelectric phase is expected to be weakened as the dimensions of the sample are reduced below some tens of nanometres [2]. However, most of the ferroelectric films of practical interest have thickness above 0.1 μm and are therefore expected to behave as 'normal' ferroelectrics. $BaTiO_3$ films as thin as 0.2 μm exhibit sharp anomalies at the phase transition temperature [67] implying that they are still ferroelectric. Nevertheless, there are many thickness- and surface-related effects which are characteristic of thin films and which can show a profound effect on film properties. From the application point of view these effects are important as they control the behaviour of the films, including polarization switching and fatigue. In this section we shall briefly discuss the effects of defects, microstructure, stress and electric fields on the dielectric permittivity and polarization–electric field (P–E) hysteresis behaviour of ferroelectric thin films. In all cases the reader is urged to consult original references for detailed discussion.

5.2. Polarization switching (hysteresis loops). Depletion and depolarization effects

5.2.1. Introduction. The most studied, and from the application point of view one of the most interesting properties of ferroelectric materials, is the polarization switching (hysteresis loop behaviour) (see section 4.4). There are important differences in the hysteresis loops measured on bulk and thin-film ferroelectrics of similar composition. The most striking difference is the magnitude of the coercive field E_C which may be as much as an order of magnitude higher in films than in bulk materials of the same composition [68]. The origins of this difference are presently not clear. In addition, loops in films are often more tilted and remanent polarization generally lower than in corresponding bulk materials. Because of the well known dependence of the properties of thin films on the preparation conditions, at least some difference in the switching properties may be attributed to different processing of thin-film and bulk materials. However, it is expected that size effects (the thickness of films) also play an important role and that mechanisms that control polarization switching in films and bulk materials may be different.

Several models of domain-wall switching, including: (i) nearby electrode nucleation of domains of opposite polarity; (ii) thermoactivated domain-wall motion; (iii) the presence of a surface dielectric layer; (iv) surface pinning of domain walls and (v) semiconductor-depletion-assisted nucleation of domains of opposite polarity have been recently critically reviewed [69]. According to this analysis, the presently available experimental results, which show a decrease of E_C with an increase in the film thickness, are consistent with models of surface pinning of the domain walls and the depletion-assisted nucleation of the walls. In the model of surface pinning of domain walls and the depletion-assisted nucleation of the walls. In the model of surface pinning of domain walls it is assumed that the origin of the coercive field is in pinning of domain walls by surface inhomogeneities [70]. This very qualitative model, which predicts that $E_C \sim 1/t$, where t is the film thickness, gives estimates of E_C which agree within an order of magnitude with experimental values. The model on the depletion-assisted nucleation of domain walls is described in some more detail below.

5.2.2. Effects of the depletion layer on the coercive field. Most perovskite ferroelectrics can be considered as semiconductors with a low mobility of free carriers [71]. When a semiconductor is brought into contact with a metal electrode, a Schotky barrier with a space charge or depletion region (a region depleted of charge carriers) and band bending is formed in the semiconductor at the interface. The depletion layer is due to different work functions of the semiconductor and the electrode, or due to a high concentration of surface states [2, 72–75], and is accompanied by a so-called built-in electric field, E_{bi}, figure 13 [74]. In thin films with a top and bottom metal electrode, a depletion layer will form at each interface. The thickness of the depletion layer in bulk materials is estimated to be a fraction of a micrometre and could thus be comparable to the thickness of films.

The model on the depletion-assisted nucleation of domain walls is based on the idea that the built-in field associated with the depletion layer is thickness dependent [75], figure 13. If the thickness t of the film is larger than double the thickness of the depletion layer ($t > 2w$) the value of the built-in field at the electrode is $E_{\mathrm{bi}} = (eNw/\varepsilon)$, where N is the concentration of free carriers, e is their charge, and ε is the dielectric constant of the ferroelectric. For very thin films (well below 1 μm) the thickness t of the film may be smaller than double the depletion layer ($t < 2w$), and the whole film becomes depleted. The experimental evidence suggests that this is actually the case in many thin films investigated today [76]. In that case the value of the built-in field at the electrode is $E_{\mathrm{bi}} = eNt/2\varepsilon$.

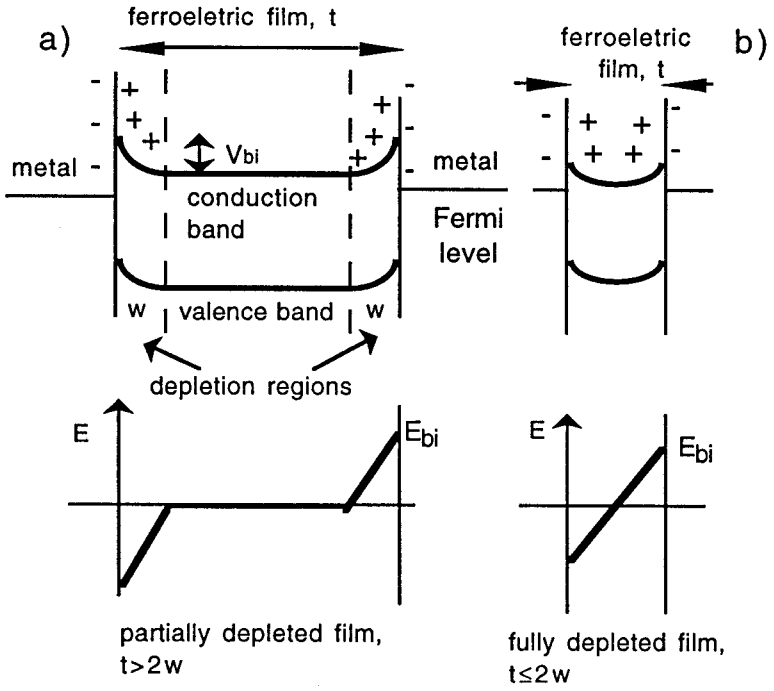

Figure 13. Schotky barriers and built-in electric field for (*a*) partially depleted ($t > 2w$) and (*b*) fully depleted ($t \leqslant 2w$) ferroelectric film in contact with metal electrodes. (For more details see [2, p 527], 159, 73, p 34].

For $t \sim 0.3\ \mu$m, $N \sim 10^{18}$ cm^{-3} and ε typical for Pb(Zr, Ti)O_3 films, the value of E_{bi} is comparable to that of the coercive field [75]. Assuming that the field necessary for the nucleation of oppositely oriented domains at the electrode, E_{cn}, is much higher than the field required to keep the walls created by nucleation moving, one finds that the film starts switching when the external field E_{ex} plus the built-in field E_{bi} are equal to E_{cn}.

The external field that satisfies this condition is the coercive field E_C and one obtains from $E_{ex} + E_{bi} = E_{cn}$ that $E_C = E_{cn} - E_{bi}$. For thicker films, which are not completely depleted, the coercive field is thus independent of the film thickness ($E_{bi} = eNw/\varepsilon$). For fully depleted films, the coercive field is thickness dependent, $E_C = E_{cn} - eNt/2\varepsilon$. This model thus predicts a decrease of E_C with film thickness for very thin films and saturation of E_C for thicker films, and is therefore in qualitative agreement with experimental results [68].

5.2.3. Effects of a depolarizing field on hysteresis loop behaviour. The tilt of the loops, figure 14, can be explained by the presence of a dielectric layer on the top of the ferroelectric [77, 78]. This layer separates the bound charges that are due to the ferroelectric polarization from the compensating charges on the electrode. The depolarizing field will thus be incompletely compensated for even if the top and bottom electrodes are shorted (see section 4.2). The depolarizing field E_d which is due to the presence of the dielectric layer is given by $E_d = -Pd/\varepsilon_d t$ where d and ε_d are the thickness and permittivity of the dielectric layer, and P and t are the polarization and thickness of the ferroelectric layer [77]. It can be shown that for $d \ll t$, the total field E_f across the ferroelectric is given by

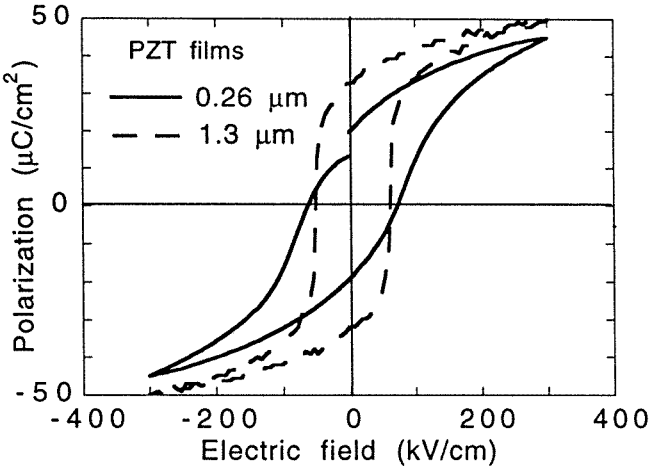

Figure 14. Comparison of ferroelectric hysteresis loops for two (111)-oriented sol-gel $Pb(Zr_{0.45}Ti_{0.55})O_3$ thin films with different thicknesses. The tilted loop is observed in the thinner film which contains a dielectric pyrochlore layer (full curve). (Film data courtesy of D V Taylor.)

[75, 77–79]:

$$E_f = E - \frac{Pd}{\varepsilon_d t} \tag{58}$$

where E is the applied field. The tilt of the loops, defined here as the slope of the measured loop at E_C, may be found from (58) as

$$\left(\frac{\partial E}{\partial P}\right)_{E_C} - \left(\frac{\partial E_f}{\partial P}\right)_{E_C} = \frac{d}{\varepsilon_d t}. \tag{59}$$

Since for the perfectly square loop of the ferroelectric layer $(\partial E_f/\partial P)_{E_C} = 0$, $[(\partial P/\partial E_f)_{E_C} \to \infty]$, the slope of the measured loop is equal to $d/\varepsilon_d t$, i.e. the loop becomes more tilted as the d/t ratio increases. The tilt of the loops can thus be taken as an indication of the presence of a low dielectric-constant ('passive') layer in series with the ferroelectric. Finally, and without going into a detailed discussion, the consistent analysis of the problem shows that the presence of a dielectric layer cannot account for the high value of the coercive field in thin films [77].

5.3. Ferroelectric (polarization) fatigue

5.3.1. Introduction. The ferroelectric fatigue is defined as the loss of the switchable remanent polarization in a ferroelectric material as a function of the number of bipolar switching cycles (figure 15). The mechanisms of the ferroelectric fatigue are presently not well understood. Both bulk and thin-film materials are susceptible to ferroelectric fatigue; in addition, suppression of the switchable polarization may be induced by treatments other than or in addition to field cycling.

In a comprehensive study of ferroelectric fatigue in (Pb, La)(Zr, Ti)O_3 (PLZT) ceramics by Jiang *et al* [80] two types of fatigue mechanisms were identified. The first mechanism is associated with microcracking. It occurred in compositions with large tetragonal lattice distortion, and in compositions near the phase boundaries in which the polarization switching

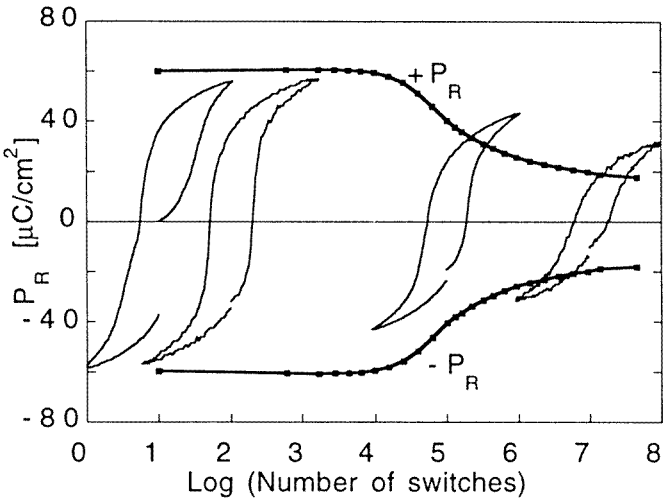

Figure 15. An example of polarization fatigue in a $Pb(Zr, Ti)O_3$ film with Pt electrodes. (Courtesy of E L Colla.)

is accompanied by field-induced phase transformation. In each case polarization switching is accompanied with large deformation of grains. The fatigue in these compositions was found to be irreversible and microcracks have been observed in the fatigued ceramics. In hot-pressed rhombohedral compositions, on the other hand, no or little fatigue was observed, which was explained by small shear distortion of the rhombohedral lattice with respect to the cubic paraelectric structure. The second mechanism was attributed to domain-wall pinning by space charges or injected charges. This type of fatigue was found to be a function of temperature. The lower fatigue rates at high temperatures were explained by the decrease of the polarization with temperature and unpinning of the domains by the driving field. The parallel study of high-quality defect-free single crystals of triglycine sulphate (TGS) showed no fatigue, consistent with the absence of defects and domain-wall pinning and the fact that polarization changes by only 180° domain switching (i.e. without an accompanying strain). The same authors have shown that the fatigue in bulk materials is dependent on the electrode material and electroding method [81], surface treatment [82], porosity and grain size [80].

Recently most of the attention in this area of research has been devoted to fatigue studies in ferroelectric thin films. From the application point of view the most interesting achievements were the discovery of the absence of significant polarization fatigue with electric field cycling in $SrBi_2Ta_2O_9$ films with metal electrodes [83] and PZT films with conducting oxide electrodes [84]. It has been shown, however, that in both cases the switchable polarization can be suppressed by illumination of the film with UV light combined with electrical field cycling or with electric field bias [85]. Another important point is that, in most cases and for most reported experimental conditions, the fatigue appears to be reversible, i.e. application of an electric field, illumination with UV light, high temperature (above T_C) anneal or combined effects of the three can nearly fully restore the initial state of the polarization. This does not mean that fatigue mechanisms by which films become permanently damaged or changed are absent or impossible; it simply indicates that in most reported studies in which fatigue is performed under usual experimental conditions the fatigue process is, at least partially, reversible. However, it was also found that rejuvenated

films do fatigue faster [86] which indicates that some sort of permanent changes, which nevertheless allow partial reversibility of the fatiguing process, may have occurred in the films fatigued by the electric field cycling. Polarization fatigue induced by microcracking and electrode delamination has also been reported [87].

The presently considered fatigue mechanisms in thin ferroelectric films include: (i) formation of a surface layer [88–90]; (ii) pinning of domain walls by defects segregated in the wall region [85]; (iii) clamping of polarization reversal by volume defects [91]; (iv) suppression of nucleation of oppositely oriented domains at the surface [92, 93]; (v) damage of electrode/film interface [87]. The role of oxygen vacancies in the fatigue process of ferroelectric thin films has been considered in several models and will be discussed below together with models of domain-wall pinning and clamping. A recent model [92, 93] which shows that, depending on the stage of fatigue and experimental conditions used, several mechanisms may play a role in the fatiguing process, will also be discussed in some detail.

5.3.2. Possible role of the oxygen vacancies. Several models of the polarization fatigue in ferroelectric thin films are based on the observation that oxygen vacancies accumulate at the film/electrode interface during field cycling [88–90, 94]. Scott *et al* [88,89] suggested that oxygen-deficient regions grow into the bulk, effectively screening part of the film from the applied field and leading to polarization loss. Another model proposed that the polarization loss is due to structural damage at the film/electrode interface due to entrapped oxygen vacancies [90]. Mihara *et al* [94] also gave evidence for the creation of oxygen-deficient layers at film/electrode interfaces in $Pb(Zr_{0.4}Ti_{0.6})O_3$ films fatigued by electric field cycling. However, their results suggest that the fatigue is due to pinning of domain walls by oxygen vacancies and not due to the presence of the interface layer. They based this conclusion on measurements of the weak-field dielectric constant as a function of DC bias electric field. At low DC bias, the permittivity of fatigued films is lower than in unfatigued films which they interpreted to be a consequence of domain-wall pinning in the fatigued films, and loss of the domain-wall contribution to the permittivity. At high DC electric fields, they found that the dielectric permittivity is nearly the same in fatigued and unfatigued samples. This is not consistent with the presence of a low dielectric permittivity surface layer in fatigued films which would decrease the weak-signal dielectric permittivity at all DC bias fields.

It has been further suggested that creation of an oxygen-vacancy-rich region at the film/metal electrode interface may lead to the formation of an n-type layer near the interface [85, 89]. The presence of this layer increases the electron injection rate in the film during field cycling. Injected electronic carriers may get trapped at the domain walls leading to domain-wall pinning and polarization suppression as discussed in the section below. Another possible role of the oxygen vacancies is to stabilize the trapping of electronic charges (and therefore to increase domain-wall pinning) through distortion of the oxygen octahedron which is caused by the presence of an oxygen vacancy [95].

The idea that oxygen vacancies may play an important role in the fatiguing process is supported by the fact that $Pb(Zr, Ti)O_3$ films with conducting oxide electrodes instead of metal ones do not fatigue under field cycling. It has been proposed that oxide electrodes act as sinks for oxygen vacancies and prevent their accumulation at the film/electrode interface [85]. A smaller concentration of oxygen vacancies at the interface would reduce injection of electronic carriers into the film, which would consequently reduce pinning of domain walls and fatigue.

Warren *et al* [86] reported that annealing of films in an oxygen-poor atmosphere may lead to polarization suppression and changes in the hysteresis loop. Original loops in films

could not be restored by electronic charge injection but could be restored by annealing in oxygen. According to Warren *et al* this mechanism of polarization suppression is attributed to the creation of oxygen vacancies which serve as pinning centres for domain walls in partially reduced films. It is interesting that a similar effect on the polarization loops was observed in single crystals of barium titanate [96].

5.3.3. Electronic charge trapping and domain-wall pinning. The model by Al-Shareef *et al* [85] is based on the idea that free electronic charge carriers pin domain walls by being trapped in the domain-wall region. The free electronic charges may be attracted to the domain-wall regions where there is a discontinuity in polarization, and thus decrease the energy of the walls. If the charges become trapped at these positions, the movement of the walls will be restricted. The charge carriers may be injected into films from the electrodes, created in the material during the field cycling or can be produced by illumination of the films by UV light [97]. The polarization fatigue process is interpreted as a dynamic competition between domain-wall pinning due to electronic charge trapping and field-assisted unpinning of the domain walls [85]. The weak fatigue in some films thus does not necessarily indicate that pinning of domain walls is absent but rather that the depinning may be as strong as the pinning. It is proposed that the unpinning may be due to a number of processes, including: (i) overcoming of the pinning forces by the cycling field; (ii) detrapping of charge carriers which are responsible for the domain-wall pinning and (iii) recombination of photogenerated or injected carriers with the trapped charge, which may unpin walls. The absence of fatigue by field cycling in $SrBi_2Ta_2O_9$ as compared with PZT with metal electrodes is then explained by: (i) a relatively small magnitude of the ferroelectric polarization (and therefore weaker trapping or smaller concentration of trapped charges in the domain-wall region); (ii) shallow electronic charge trapping centres (holes and electrons associated with Bi^{+4} and Ta^{+4}, respectively) which may be easily detrapped by the field and (iii) possibly lower accumulation of oxygen vacancies at the electrode/film interface due to the layer structure of this material. Absence of fatigue in PZT films with conducting oxide electrodes compared with films with metal electrodes is explained by a lower concentration of injected carriers and/or by a lower concentration of oxygen vacancies, as outlined in the previous section.

5.3.4. Suppression of nucleation of oppositely oriented domains at the surface. This model is based on a comprehensive study of the fatiguing process in $Pb(Zr, Ti)O_3$ films with Pt-electrodes produces by sol-gel and metal oxide chemical vapour deposition (MOCVD) techniques [92, 93, 98, 99]. It was observed that under fast switching conditions the polarization measured as a function of the number of cycles shows three distinct regions, as shown in figure 16.

In region I, which is dependent on the processing and fatiguing conditions, the polarization behaviour is nearly independent of the frequency and amplitude of the electric field. The fatigue in this region is noncumulative; if the sample is originally fatigued with field E_1 and then fatigued with field $E_2 > E_1$, the effects of the two fatiguing processes do not add up. The degradation provoked by the first fatigue is removed and replaced by the higher field fatigue. In region II the self-rejuvenation of the polarization takes place. The authors report that the self-rejuvenation is due to an increase of switching polarization and is not caused by the contribution from the leakage current. After reaching the maximum recovered polarization decreases with further cycling (region III). The number of cycles at which the maximum of recovered polarization occurs, N_{max}, depends on the field strength (N_{max} decreases with an increase in the field) and total duration of the fatiguing pulses.

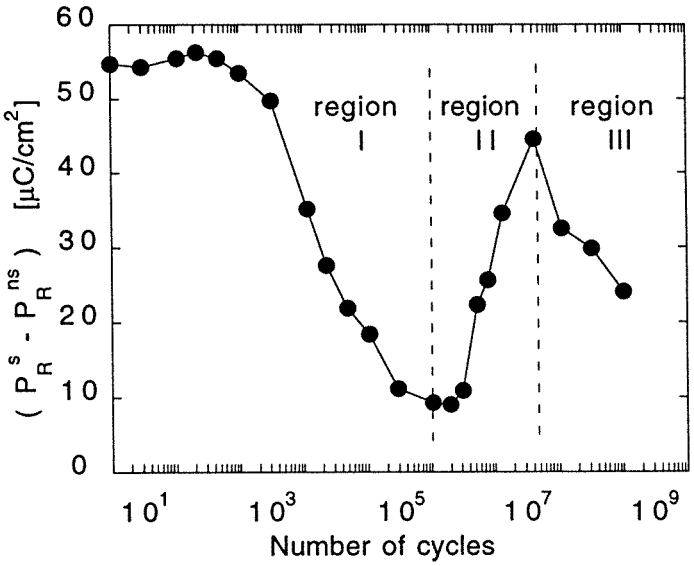

Figure 16. Polarization fatigue in a MOCVD $Pb(Zr_{0.53}Ti_{0.47})O_3$ film showing initial fatigue (region 1), self-recovery (region II) and degradation (region III). Plotted on the vertical axis is the difference between switchable and nonswitchable polarization (see [93]).

The fatigue behaviour in region I is explained by the local blocking of the nucleation sites of oppositely oriented domains by the space charge produced by the strong switching electric field. In other words, nucleation of oppositely oriented domains in some parts of the fatigued film becomes strongly inhibited. This process of polarization suppression can be reversed by, for example, high enough electric fields. According to the model, the fatigued film contains large, nearly single-domain regions with locked polarization rather than many domain walls pinned by defects, as proposed by models of domain-wall pinning (see section 5.3.3). The method used to distinguish between these two possibilities was to compare weak-signal dielectric permittivity in fatigued and unfatigued films as a function of DC bias field [99,100]. Unfatigued films are expected to be free of domain walls (completely switched) at large DC bias and only lattice effects can contribute to the dielectric permittivity. It was found that the dielectric permittivity at large DC fields in fatigued and unfatigued states is nearly identical. This implies that fatigued films indeed contain large single-domain regions with locked polarization and with unchanged weak-signal dielectric properties. Using the technique of atomic force microscopy, Colla *et al* [92] have shown that fatigued films indeed possess large regions with locked polarization. If the fatigue process was due to the pinning of domain walls, according to the authors, the dielectric permittivity at large DC bias would be higher in fatigued than in unfatigued films. The reason for this is that both lattice and weak-field oscillations or bending of domain walls would contribute to the permittivity of fatigued films (anisotropy in dielectric permittivity due to possible different orientations of domains not being taken into account). Evidence presented by Colla *et al* [100] suggests that the fatigue by domain-wall pinning can be observed in films fatigued at a low frequency ($\sim$1 mHz), giving enough time for slowly moving defects to diffuse into the domain-wall region.

The recovery of the switchable polarization in region II is explained by a process which is independent of the fatigue and which leads to a local increase in the conductivity of the

film in regions around the blocked nucleation sites [101]. The self-rejuvenation probably occurs when the local increase in the conductivity is large enough so that the field can remove partly or completely the space charge which blocks the nucleation sites. Indeed, the self-rejuvenation was found to be strongly dependent on the amplitude of the fatiguing field and on the total duration of the fatiguing pulses. The observed slight increase in the total conductivity of the film at the point of rejuvenation is consistent with an increase in the local conductivity. The increase in the local current and the high current density eventually destroy locally the film/electrode interface, leading to a decrease of the effective electrode area and polarization suppression (region III) due to film degradation. As an indication that the interface has indeed changed in region III, a drop in the weak-signal dielectric permittivity at large DC bias fields has been observed.

5.4. Effects of external fields on ferroelectric properties

5.4.1. Stress effects. One of the particular features of thin films is the presence of large two-dimensional stress (or strain) in the plane of the film. The origin of this stress is in the mismatch between the thermal expansion coefficients of the film, electrodes and substrate. The exact values of the stress are difficult to predict because stress relaxation mechanisms due to, for example, film/electrode interface and imperfect film microstructure are usually not known. Simple estimates [102, 103] as well as experimental results [104] show that these stresses may be on the order of several hundreds of MPa. The presence of the stresses can affect properties of ferroelectrics in many ways. Stress may decrease the irreversible contribution of non-180° domain walls to the properties [39, 105], shift the phase transition temperature [102], change the order of the phase transition [55, 58, 59], increase diffuseness (broadness) of the phase transition [102], change the sequence of phase transitions and even induce new phases in the material [58, 59].

The LGD thermodynamic approach (see section 4.7) is particularly useful in studying field effects on ferroelectric phase transitions. Let us illustrate this using, for example, a one-dimensional ferroelectric with second-order phase transition, by demonstrating the effect of the stress on the transition temperature. The elastic Gibbs energy is given by equation (46). If the external stress is not zero, then expression (47) becomes

$$E = \left(\frac{\partial G_1}{\partial D}\right) = \alpha_1 D + \alpha_2 D^3 + \alpha_3 D^5 + 2QXD = \alpha_1' D + \alpha_2 D^3 + \alpha_3 D^5 \tag{60}$$

where $\alpha_1' = \alpha_1 + 2QX$. Following the same procedure as in section 4.7, the expression for polarization (51) in the presence of external stress becomes

$$P_S^2 = -\frac{\alpha_1'}{\alpha_2} = -\frac{\alpha_1 + 2QX}{\alpha_2} = -\frac{T - (T_0 - 2QXC)}{\alpha_2 C}. \tag{61}$$

The phase transition temperature is thus shifted (depending on the sign of X) by $2QXC$. For the values of Q and C typical for ferroelectric materials ($Q = 0.1$ m^4 C^{-2}, $C = \varepsilon_0 10^5$ F °C^{-1} m^{-1}) we see that 100 MPa stress will shift the transition temperature by approximately 20 °C.

In the case of thin films, two-dimensional clamping of the film requires the use of the appropriate free energy function. To obtain the free energy appropriate for the general case of a thin single-domain film epitaxially grown on a thick substrate, Pertsev *et al* [59] proposed the following Legendre transformation of the elastic Gibbs function:

$$\tilde{G} = G_1 + x_1 X_1 + x_2 X_2 + x_6 X_6. \tag{62}$$

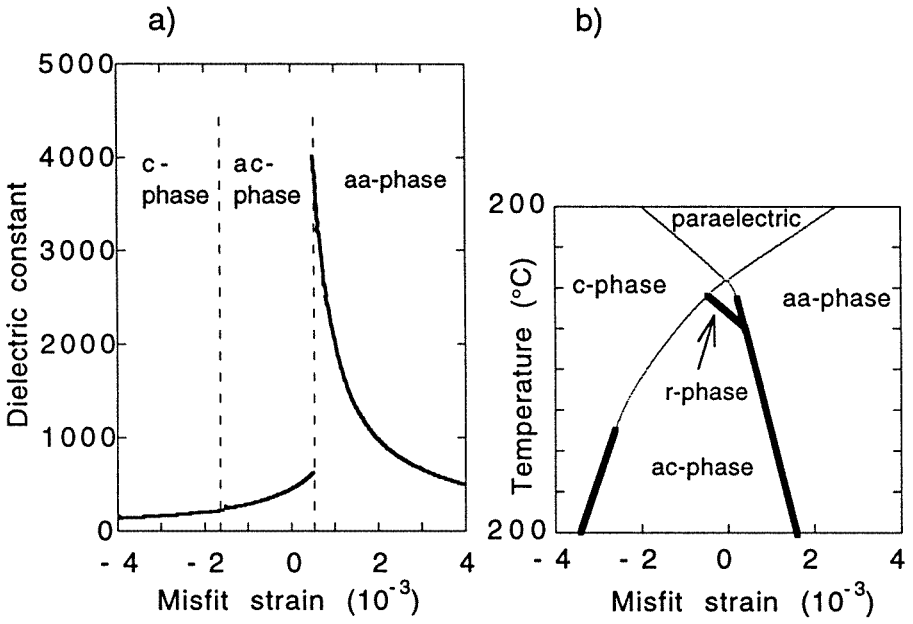

Figure 17. (*a*) Dielectric permittivity at room temperature and (*b*) phase diagram for (001) single-domain $BaTiO_3$ film epitaxially grown on different cubic substrates, as a function of misfit strain. The second- and first-order phase transitions are shown by light and heavy curves, respectively. c, r, aa and ac identify the orientation of polarization in each phase. (After [59].)

This form of the free energy is based on the assumption that strains x_1, x_2, and x_6 in the plane of an epitaxially grown film are completely controlled by the substrate. Likewise, stresses X_3, X_4 and X_5 are taken to be zero on the free surface of the film. For single-domain films internal fields are homogeneous and these conditions hold throughout the film. Exact treatment of the problem applied to $BaTiO_3$ and $PbTiO_3$ thin films allows construction of the phase diagrams as a function of the 'misfit' strain. It was shown by Pertsev *et al* [59] that two-dimensional clamping of these films not only shifts the phase transition temperature, but also changes the order of the phase transitions (they become second order) and may even induce new phases. Calculations of the dielectric permittivities and piezoelectric coefficients as a function of the misfit strain, showed that one can expect anomalously high intrinsic response at certain values of the misfit strain (figure 17). For the treatment of the similar problem in barium titanate Desu *et al* [58] used another free energy expression arriving at similar results.

5.4.2. Permittivity–electric field (ε–E or C–V) loops. Dielectric permittivity versus electric field (or capacitance C versus voltage V) loops are often used in the characterization of ferroelectric materials. Typical behaviour is shown in figure 18. Measurements of ε–E (or C–V) curves are usually made by applying simultaneously on a sample a DC field which changes as a step-like function and an AC voltage of relatively high frequency (1 kHz or above) and small amplitude. The AC voltage is used to measure the capacitance which is then plotted as a function of the DC bias field, giving a C–V graph. Initial rise in the permittivity with DC field is probably due to increased movement of the domain walls which become 'free' from defects which lock them at zero-DC field [106] and due to partial

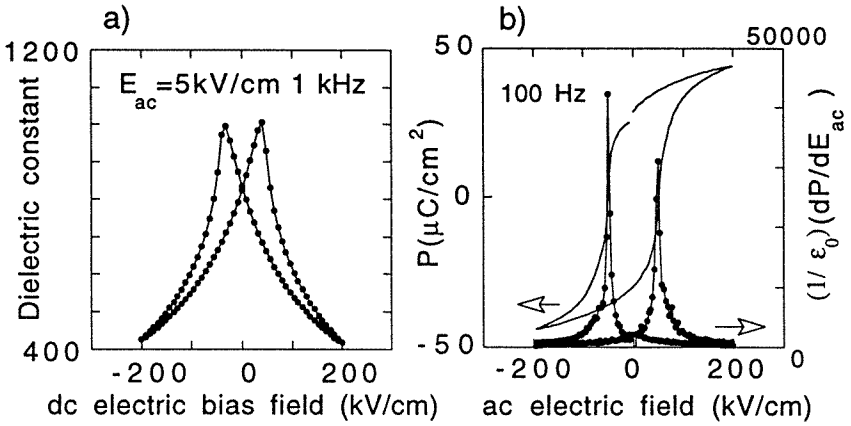

Figure 18. (*a*) Dielectric permittivity of a (111)-oriented, 1.3 μm thick $Pb(Zr_{0.45}Ti_{0.55})O_3$ film as a function of DC electric field bias. (*b*) P–E hysteresis loop of the same film and derivative dP/dE as a function of an AC electric field. ε–E_{DC} and dP/dE loops are comparable only at decreasing saturating fields, where the polarization drops from saturation towards a remanent value. (Experimental data courtesy of D V Taylor.)

switching of some domains whose coercive field happens to be small enough and which can be switched by the DC + AC field combination. The maximum in the ε–E curve appears in the vicinity of the coercive field for the P–E hysteresis when most of the domains switch and the material appears to be dielectrically very 'soft'. At high DC fields, the permittivity decrease reflects two processes: (i) decrease in the number of domains as they become aligned with the field (ideally the sample becomes a single domain and only lattice contributions are present) and (ii) inhibition of the movement of residual domain walls by the DC field [106]. It is possible, however, that small oscillations or bending of residual domain walls under the AC field can still occur even at very large DC fields, contributing to the dielectric permittivity [100]. In any case, the total domain-wall contribution to the permittivity at high DC bias becomes reduced with respect to the low DC bias fields.

An illustration how ε–E curves can be used to obtain information on various domain-wall processes in films is illustrated in reports by Mihara *et al* [94] (see section 5.3.2), Wouters *et al* [107] and Colla *et al* [100] (see section 5.3.4). It is interesting that ε–E loops in ceramic ferroelectrics can show two distinct peaks [108]. This is explained by different coercive fields for 180° and non-180° domains. The absence of a second peak in ε–E curves in thin films could thus be an indication of limited switching of non-180° walls in most thin films. This is in agreement with x-ray diffraction studies of the switching process in tetragonal Pb(Zr, Ti)O_3 films with grain size below 1 μm, which did not indicate any significant switching of 90° domain walls in examined films [109, 110]. Another structural study [111] of the switching process in tetragonal films with composition $Pb(Zr_{0.20}Ti_{0.80})O_3$ suggests, however, a substantial 90° domain-wall switching. The discrepancy may be due to different field levels used in the two studies or different grain size in the films [110].

The permittivity–DC field curve, determined as described above, is physically not identical to the curve which is obtained by plotting the derivative of P–E hysteresis loop ($\varepsilon = \partial P/\partial E$) measured as a function of the AC field. The difference is that P–E hysteresis loops are generated with a strong ($> E_C$) AC field with the frequency on the order of 100 Hz. Differential permittivity is plotted as a function of the instantaneous value of the AC field with amplitude $> E_C$ (see figure 18(*b*)); in ε–E curves, permittivity is measured with a

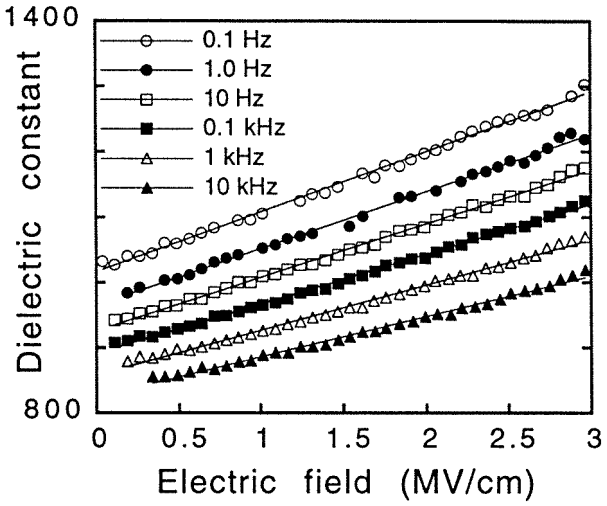

Figure 19. Dependence of the dielectric constant of a (111)-oriented, 1.3 μm thick $Pb(Zr_{0.45}Ti_{0.55})O_3$ thin film on the amplitude of the AC electric field for different frequencies. (Courtesy of D V Taylor, for details see [112].)

high-frequency AC field with subswitching amplitude, applied in addition to the DC field, and plotted as a function of the DC field (figure 18(*a*)). The values of the differential and weak-field dielectric constant are similar only at saturating fields, when polarization decreases from saturation towards a remanent value.

5.4.3. Dependence of the dielectric permittivity on the amplitude and frequency of the subswitching field. Extrinsic processes, such as displacement of defects and domain walls, are largely responsible for the field and frequency dependence of the properties of ferroelectric materials. Field-induced changes in the intrinsic (lattice) properties become important only at very large fields which are not of interest for this discussion. Thus, the studies of the field and frequency dependence of material properties may give valuable information on the nature of extrinsic mechanisms that operate in the material. On the other hand, knowledge of this dependence is essential for device modelling.

Relatively few studies have been devoted to the behaviour of the dielectric permittivity in ferroelectric films at low to moderate (subswitching) fields. Figure 19 shows typical dependence of the dielectric permittivity in $Pb(Zr, Ti)O_3$ thin films [112] on the amplitude of the AC field (in the absence of a DC bias). The field dependence of the permittivity in those films was analysed in the framework of the Rayleigh dynamics of domain walls, which is described in more detail in section 6.4.4. The linear dependence of the permittivity on the field amplitude (figure 19), may be attributed to the pinning of domain walls on randomly distributed defects. The linear decrease of the permittivity with the logarithm of driving field frequency (figure 20), also indicates that the extrinsic component of the dielectric permittivity is dominated by domain-wall pinning processes [112].

5.5. Grain-size effects

Perhaps the best known example of the effects of microstructure on the properties of polycrystalline ferroelectric materials is the grain-size dependence of the dielectric

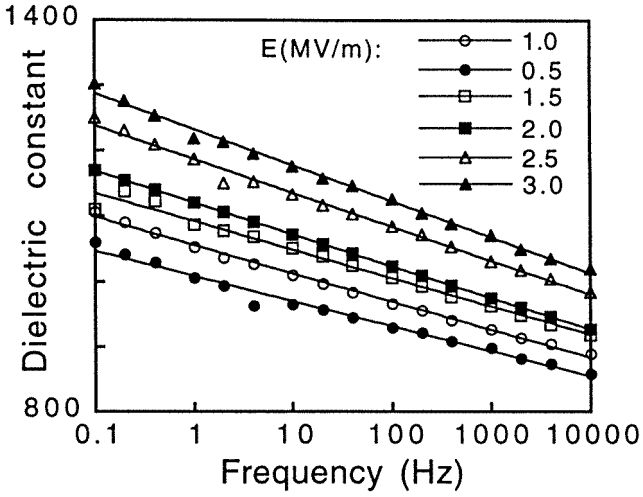

Figure 20. Dependence of the dielectric constant of a (111)-oriented, 1.3 μm thick $Pb(Zr_{0.45}Ti_{0.55})O_3$ thin film on the frequency of the AC electric field for different field amplitudes. (Courtesy of D V Taylor, for details see [112].)

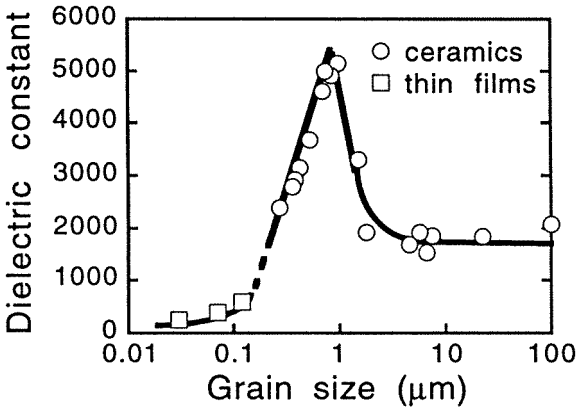

Figure 21. Dielectric constant of $BaTiO_3$ ceramics and thin films for samples with different grain size. (After Waser [76] and Arlt *et al* [115].)

permittivity in barium titanate ceramics [76, 113–116] and thin films [76] (figure 21). The complexity of the phenomenon is clearly indicated by the fact that even after more than 30 years of research the origins of the anomalously high permittivity in fine-grained barium titanate ceramics are still not well understood. Several models, including the presence of internal stresses in fine-grained ceramics, which are due to the absence of 90° domain walls [113], increased domain-wall contributions to the dielectric response in fine-grained ceramics [115, 116], shifts of the phase transition temperatures with grain size (see [76] for details) have been considered. Recent results have shown that piezoelectric response in barium titanate ceramics also shows a strong dependence on both the grain size and externally applied compressive pressure [39, 105].

The critical grain size below which tetragonal deformation in barium titanate disappears and materials becomes cubic is reported to be below 0.1–0.2 μm [117]. This appears to be

in agreement with the absence of a clear sharp maximum in the temperature dependence of the permittivity in films with thickness of about 0.25 μm reported by Hayashi [118] and Waser [76]. The maximum is expected at the ferroelectric–paraelectric phase transition and in single crystals of barium titanate occurs around 130 °C. Nevertheless, the films examined by Hayashi *et al* showed ferroelectric hysteresis loops. In contrast to the work by Hayashi *et al*, some earlier studies [67] showed that $BaTiO_3$ films as thin as 0.02 μm exhibit a sharp peak in permittivity around 100 °C as well as the ferroelectric hysteresis loop. These results indicate that the apparent grain-size (or film-thickness) dependence of the properties may sometimes be a secondary effect and that some other process controls the behaviour of the material. From the processing point of view it is usually difficult and often impossible to change only one material parameter (grain size or thickness) and keep all others unchanged. In conventionally processed PZT ceramics, for example, chemical homogenization (Ti/Zr distribution within grains and from grain to grain) which can strongly affect the properties in the vicinity of the morphotropic phase boundary (see section 6.2) appears to be closely linked to the grain growth [119].

In $Pb(Zr, Ti)O_3$ films Tuttle *et al* [110] reported the absence of 90° domain walls in films with grains less than 0.1 μm. Single 90° domain walls are observed in grains ranging from 0.2 to 1 μm, and only for grains larger than 1 μm are multiple 90° domain walls observed. Such behaviour is qualitatively consistent with observations that domain width decreases with a decrease in the grain size [19, 120]. The absence of the 90° domain walls in films with very fine grains is expected to affect the electromechanical properties of films both at subswitching fields and fields with amplitude $> E_C$. It is interesting that the study by Cao and Randall [120] on $Pb(Zr, Ti)O_3$ ceramics indicates that the domain switching process involves transgranular cooperation of domains. Clearly, if this is indeed the general case, the quality of grain boundaries, presence of intergranular phases and porosity will affect domain-wall switching.

5.6. Ageing and internal bias fields in ferroelectric materials

Ageing is defined as a change of the materials properties with time, and is provoked by temperature change, or by application of strong external fields [31, 73]. In ferroelectric materials the ageing of a property m (for example, dielectric permittivity, piezoelectric and elastic coefficients) with time t can often be described over several decades of time (minutes to days) by the following logarithmic dependence [73]:

$$m(t) = m(t_0) + A \log(t/t_0) \tag{63}$$

where t_0 is an arbitrary point in time when measurements were started. Constant A, which indicates the 'ageing rate', can be either positive or negative [11]. Relation (63) does not hold universally [11, 121] and clearly not for very long times (m would become infinite or zero). Most models relate ageing to a gradual change of the domain configuration with time. The origin of the change may be in internal stresses which build up in polycrystalline materials each time configuration on non-180° domain walls is altered. The stresses are relaxed with time by reconfiguration of domains into new equilibrium states [11]. Alternatively, domain-wall configuration may stabilize with time due to the presence of defects in the material [41, 122]. Several models of defect-induced stabilization of the domain structure have been proposed. According to Carl and Haerdtl [41], these models can be tentatively classified according to the following mechanisms.

The first mechanism is associated with volume effects. Anisotropic elastic and/or electric defects within domains are at first randomly oriented. (Elastic defects are associated with

lattice distortion, due to the presence of vacancies or substitutions with atoms of different size.) In the course of time these defects will slowly reorient into new, energetically more favourable positions, which are dictated by the direction of the spontaneous polarization or strain tensor. Once defects are aligned with the direction of the spontaneous polarization and/or deformation tensor, subsequent reorientation of the polarization (or strain tensor) and displacement of domain walls by external fields become very difficult. This happens because any change in the polarization or spontaneous strain direction by an external field will now require reorientation of aligned defects, which may require considerable energy and time. It is said that the domain walls are clamped by defects.

The second mechanism is related to diffusion of defects into domain walls and consequent stabilization of the wall position. The driving forces for defect displacement may be neutralization of stresses or compensation of electric charges in the wall region. The defects act as pinning centres for walls restricting their movement. Since both mechanisms restrict domain-wall displacement, the domain-wall contribution to the properties as well as losses associated with domain-wall displacements are decreased. The third mechanism is related to the presence of space charges in the grain boundary regions, for example, due to the presence of second phases or dopants segregated in the grain boundary region. The space charges will create a field which will stabilize domain-wall configuration, once it reaches its equilibrium state in the course of time. In this mechanism, the whole grain becomes biased in a certain direction, but small oscillations of the domain walls are still possible [41].

Common for all mechanisms outlined above is the presence of internal bias fields in aged samples i.e. in samples with stabilized domain structure. The internal bias field acts as an additional coercive field for reorientation of aligned defects. The internal bias field is manifested by shifts of ferroelectric hysteresis loops along the field axis, or constriction of the loop (figure 22). A shift of the loop occurs if defects are preferentially oriented in approximately the same direction in the whole sample; it is observed, for example, in poled and aged polycrystalline materials where the poling direction is the preferential direction of defect alignment. Constricted loops occur when defects and internal fields are randomly distributed in the sample. It appears as though the sample exhibits two loops, one with negative and the other with positive internal bias field. Constricted loops are observed in thermally depoled, aged ceramics [41]. Samples may be de-aged, and loops centred by thermal treatment or by high-field cycling. Both processes randomize the orientation of defects, however, after the treatment, the ageing process and build-up of internal fields will start again.

The ageing process and origin of internal fields are now rather well understood in acceptor-doped ferroelectrics [57, 122]. Robels and Arlt [122] gave a quantitative model of ageing in acceptor-doped ferroelectric ceramics. The origin of ageing is interpreted as a slow increase of the domain-wall force constant (see section 6.4.2) by the relaxation of dipolar defects. The defect dipole consists of an acceptor ion on the Ti site and an oxygen vacancy, $V_{\mathrm{O}}^{\bullet\bullet}$. The orientation of the defects takes place through diffusion of oxygen vacancies [123]. They showed that the increase in the force constant is proportional to the internal field, E_i, and that the domain-wall contribution to the properties is inversely proportional to E_i. The internal field increases with time (with ageing) as described by equation (63) and domain-wall contributions decrease with time in a similar fashion. De-ageing of material by electrical treatment leads to a decrease of the E_i which can be described by a simple exponential law ($\sim \exp(-t/\tau)$ [41, 122]. Domain-wall contributions to the properties then increase in a similar exponential manner. It is interesting that the model predicts that elastic defects will shift the mechanical (strain–stress) hysteresis loop. Clearly, more than one

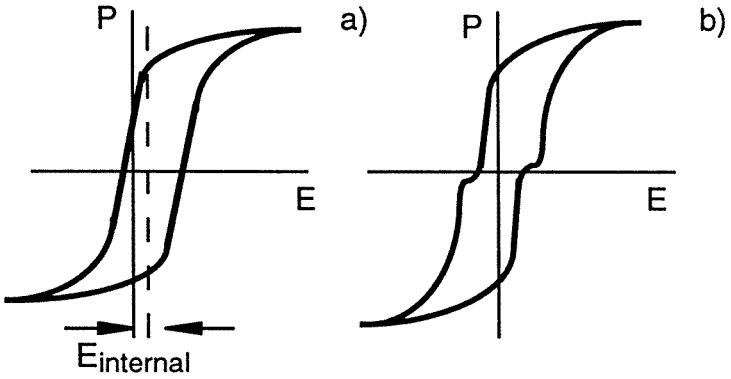

Figure 22. (*a*) Shifted and (*b*) constricted hysteresis loops in ferroelectrics. See text for an explanation.

ageing process can operate in a material at the same time.

There are few reports on the ageing behaviour of the weak-signal properties of ferroelectric thin films [124, 125]. Kholkin *et al* [125] showed that the dominant mechanism in the ageing of the piezoelectric properties of tetragonal $Pb(Zr, Ti)O_3$ films is depolarization of the films rather than suppression of the domain-wall motion. Shift and deformation of the hysteresis loops (large signal properties) in thin films have been studied by several groups. Pike *et al* [126] found that the donor-doped $Pb(Zr, Ti)O_3$ films cooled from the processing temperature in a reducing atmosphere exhibit a similar shift of the hysteresis loops along the field axis as acceptor-doped materials. The shift of the loops is interpreted in terms of the asymmetric distribution of oxygen vacancies and trapped electrons. Lee *et al* [127] reported that the shift and constriction of loops in their $Pb(Zr, Ti)O_3$ films can be removed by thermal annealing. It is suggested that the origin of the loop deformation is in defects and space charges which are formed in the films by sputtering and the reactive ion etching process used for electrode patterning. Time dependence of internal field or other properties was not reported in those studies.

5.7. Retention, endurance and imprint

Recently the concentration of the research efforts in the area of ferroelectric materials was mainly on large signal polarization response of ferroelectric thin films. The main drive behind this interest is ferroelectric memory application. Certain terminology has emerged which refers to the condition of the devices and which is related to material behaviour. From the device point of view it is common to use the terms ‘endurance’ and ‘retention’, as rough equivalents for fatigue and ageing processes discussed above. Endurance may be defined [128] as the ability of a device to retain a given level of electric signal from the ferroelectric memory cell as a function of accumulated rewrite cycles. Retention may be defined as the ability of the device to retain a given level of electric signal from the ferroelectric memory cell after a given time period from the write operation. Another term often used is ‘imprint’. Imprint is the tendency of a ferroelectric memory element to develop a preferential state under certain conditions; after prolonged storage periods in the same state or many rewrites into the same state it may become difficult or impossible for the element to retain different data for a significant period of time [129].

It is obvious that the retention, endurance and imprint are closely related to the

processes which lead to ageing and fatigue of materials, described in sections 5.3 and 5.6. Understanding of the mechanisms which control device performance will require detailed knowledge of the domain-wall processes, role of defects, effects of microstructure and electric and mechanical fields on the properties of ferroelectric films.

6. Piezoelectric properties of ferroelectric materials

6.1. Introduction

Interest in the piezoelectric properties of ferroelectric materials stems from very high piezoelectric coefficients in many ferroelectrics and the fact that ferroelectric materials may be prepared in a polycrystalline form and still, after electrical poling, exhibit large piezoelectricity (see section 4.3). The value of the piezoelectric coefficients in ferroelectric materials at room temperature ranges from several pC N^{-1} in the $Sr_2Nb_2O_7$ family of layer structure perovskites [130] to more that 2000 pC N^{-1} in single crystals of relaxor-based ferroelectrics [12], covering three orders of magnitude. Preparation in the polycrystalline (ceramic or thin-film) form has the additional advantages that the composition may be more easily adjusted than when preparing single crystals, so that materials with a very large range of properties may be obtained. An example which illustrates this well is a solid solution of lead titanate ($PbTiO_3$ or PT), and lead zirconate ($PbZrO_3$ or PZ) which are soluble in all proportions. The resulting material, $Pb(Zr_xTi_{1-x})O_3$ or PZT, is after quartz the most widely used piezoelectric.

6.2. PZT solid solution and the morphotropic phase boundary

A schematic of lead zirconate titanate, $PbZrO_3$–$PbTiO_3$ phase diagram, is shown in figure 23 (see also [11, 31]). Compositions are abbreviated by $100x/100(1-x)$ PZT where $100x/100(1-x)$ indicates in per cent the Zr/Ti ratio in the solid solution. Zr and Ti are randomly distributed over B-sites of the perovskite structure ABO_3 (see figure 4). The structure of the high-temperature paraelectric phase is cubic. Titanium-rich compositions transform into tetragonal perovskite structures whereas the phase transformation in Zr-rich compositions is more complex. At low Ti content ($x > 95\%$) and at room temperature the structure is orthorhombic and for $x < 90\%$ the structure is rhombohedral, with another phase transition from a high- to a low-temperature rhombohedral phase, as shown in figure 23. The rhombohedral and tetragonal structures in the middle of the diagram are ferroelectric.

From the application point of view the most interesting compositions lie near the centre of the phase diagram, where tetragonal and rhombohedral phases are separated by a boundary which is nearly independent of temperature. The composition of this so-called morphotropic phase boundary (MPB) is approximately 52/48 at room temperature. The piezoelectric coefficients, electromechanical coupling coefficients, dielectric permittivity and remanent polarization measured on ceramic samples reach a peak in the region of the morphotropic phase boundary, figure 24 (not necessarily at the same composition [31]), which explains why these compositions are technologically so interesting. Good-quality single crystals of PZT with compositions in the middle of the phase diagram are not available, therefore comparable measurements could not be made on single-domain single crystals. Calculations using the thermodynamic phenomenological theory (section 4.7) have shown, however, that a peak in the piezoelectric coefficients and dielectric permittivity should be expected at MPB in monodomain single crystals [46]. The important exception is the behaviour of the polarization for which theoretical calculations do not predict a peak in single crystals

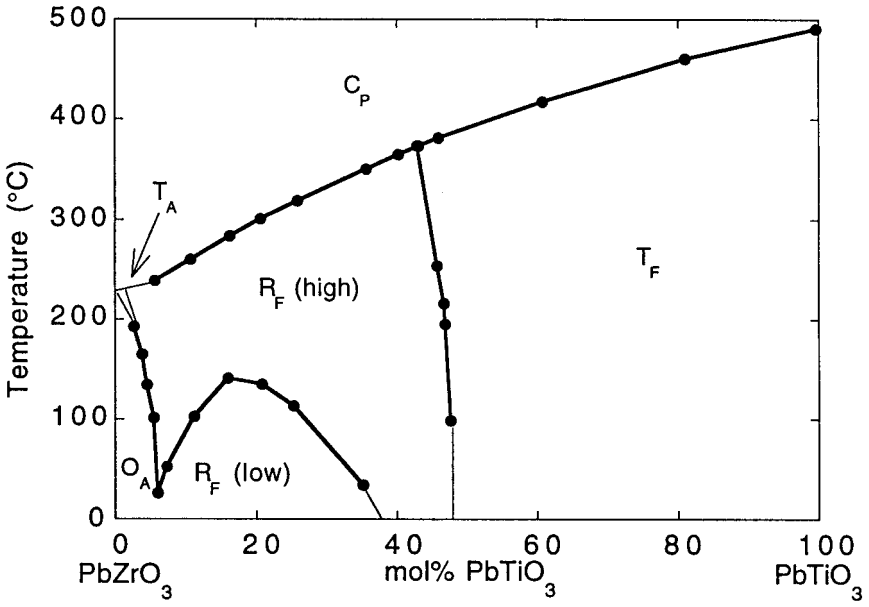

Figure 23. Phase diagram of $Pb(Zr, Ti)O_3$ solid solution showing the morphotropic phase boundary in the middle of the diagram separating tetragonal and rhombohedral ferroelectric phases. The subscripts A and F stand for antiferroelectric and ferroelectric phases, and the letters C, T, R and O for cubic, tetragonal, rhombohedral or orthorhombic phases. (After [31].)

at MPB. The results of the thermodynamic calculations have been recently confirmed by experimental study of the properties of single-crystal (epitaxial) PZT thin films [131] which clearly showed a peak in the permittivity but not in the polarization at MPB. Properties of random-oriented polycrystalline PZT thin films [132] are in qualitative agreement with results obtained on bulk ceramics.

The maximum polarization in the vicinity of MPB in polycrystalline materials is explained by the ease with which domains may be reoriented at compositions close to MPB. There are six equivalent polar axis in the tetragonal state corresponding to the (100), (−100), (010), (0−10), (001) and (00−1) directions of the cubic paraelectric phase giving a total of six domain states with 90° and 180° walls (see section 4.2). Distortion in the rhombohedral phase is along the body diagonal of the cubic state giving rise to eight possible domain states: (111), (−111), (1−11), (11−1), (−1−11), (−11−1), 1−1−1), (−1−1−1) with 180°, 109° and 71° domain walls. AT MPB, the free energy of the rhombohedral and tetragonal phases are equal and it is probable that the electrical poling field may easily switch between tetragonal and rhombohedral domain states. There are thus effectively 14 available directions along which polarization may be reoriented by the poling field, leading to a large remanent polarization for compositions near the MPB. The large remanent polarization at MPB in randomly oriented PZT also helps to increase the peak in the piezoelectric coefficients at MPB. Other interpretations of the origin of the peak in the properties of PZT at MPB have been proposed [133, 134].

The morphotropic phase boundaries are present in many solid solutions and of particular interest are compositions based on relaxor ferroelectrics such as $Pb(Zn_{1/3}Nb_{2/3})O_3$–PT and $Pb(Mg_{1/3}Nb_{2/3})O_3$–PT [12]. The largest piezoelectric coefficients in these materials are observed on the rhombohedral side of the MPB, and in single crystals in the (001) direction

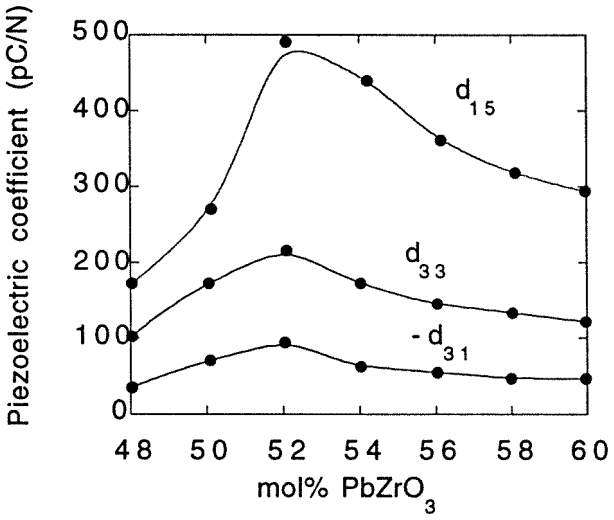

Figure 24. Piezoelectric coefficients of $Pb(Zr, Ti)O_3$ ceramics as a function of composition in the vicinity of the morphotropic phase boundary. (After [31].)

which is not coincident with the polarization direction (111). Mechanisms of the large electromechanical activity in these materials are presently not well understood.

6.3. 'Soft' and 'hard' PZT compositions. Effect of defects

PZT is rarely used in a chemically pure form. Ceramics and thin films are usually doped with the goal of tailoring the properties for specific applications [31]. Whereas the range of the properties obtainable by doping is very broad, most of the compositions of a practical interest fall into categories of so-called 'hard' and 'soft' PZT. 'Hard' compositions are obtained by acceptor doping either by replacing Pb with monovalent cations such as K^{+1} or by replacing (Zr,Ti) with acceptors such as Fe^{+3}. For simplicity we refer to *B*-site replacement as replacement of Ti. The compensating defects in this case are oxygen vacancies, $V_O^{\bullet\bullet}$. Assuming that the oxygen vacancies are doubly charged the formula of the material doped with y mol of Fe^{+3} becomes

$$Pb(Zr^{+4}_{1-x}Ti^{+4}_{x})_{1-y}Fe^{+3}_{y}O_{3-y/2}. \tag{64}$$

Oxygen vacancies can move in the oxygen octahedra network even at temperatures below T_C leading to a relatively low stability of the $2Fe^{-1}_{Ti}$–$V^{\bullet\bullet}_O$ defect dipole direction. The defect dipoles will tend to align themselves in direction of the polarization vector within domains, and this alignment will stabilize the domain structure (for details see section 5.6 and [57, 123, 135]). A consequence of the stable domain-wall structure is a high apparent coercive field (see section 5.6 [41]) and more difficult poling and depoling of ceramics (hence the name 'hard'). Acceptor doping increases the conductivity of PZT but the dielectric loss measured in the kHz region is lower than in undoped ceramics. The reason for this is that a significant part of the total measured loss is due to domain-wall motion, which is reduced in 'hard' ceramics [31].

Donor dopants such as La^{+3} in place of Pb and Nb^{+5} in place of (Zr,Ti) are compensated for either by electrons or doubly negatively charged lead vacancies V''_{Pb}. For y-mol Nb the

composition may be expressed as

$$Pb_{1-y/2}(Zr^{+4}_{1-x}Ti^{+4}_{x})_{1-y}Nb^{+5}_{y}O_3. \tag{65}$$

Donor-doped PZT are called 'soft' and exhibit high dielectric loss, low conductivity, low coercive field, are easy to pole and depole and possess high piezoelectric coefficients [31]. Examination of the perovskite structure ABO_3 (figure 4) may give us a clue as to why donor–cation vacancy pairs do not have a 'hardening' effect in PZT. In the perovskite structure, cations are surrounded by the network of oxygen octahedra and are separated from the neighbouring cations of the same kind (A or B site) by an entire unit cell (approximately 0.4 nm) making the movement of cations very difficult. Oxygen sites on the other hand are about 0.28 nm apart, adjacent one to another and may thus move more easily. These simple arguments may explain intuitively why V''_{Pb}-donor pairs do not have a hardening effect on PZT. However, there is presently no good explanation for the mechanisms responsible for the softening effect of donors in PZT [23].

It appears that the solubility of donors in PZT ceramics is higher than the solubility of acceptors [41]. Whether the same solubility limits are valid for thin films is presently not clear due to a lack of systematic studies.

6.4. Extrinsic piezoelectric response

6.4.1. Introduction. As already mentioned in section 4.5, movement of domain walls and defects under external electric and mechanical fields may contribute to the piezoelectric, dielectric and elastic response of materials and is often the major factor responsible for the frequency, field and temperature dependence of the properties [53, 136, 137]. In principle, the intrinsic lattice response, even in polycrystalline materials, may be determined from the LGD theory as outlined in section 4.7 (see for example [48]). The study of extrinsic contributions is much more difficult, especially in real polycrystalline materials because a detailed knowledge of the domain-wall structure, nature of defects present, and their possible interaction with domain walls is often lacking. Most of the reports in the literature are concerned with dielectric and to a lesser extent elastic properties (see for example [138]). In this section we shall give an overview of recent developments in the description of extrinsic contributions to the piezoelectric response of ferroelectric materials.

6.4.2. Contributions to material properties from domain-wall vibrations. A phenomenological model of vibrating 90° domain walls in electric and mechanical fields was proposed by Arlt and co-workers in a series of papers [52, 116, 139]. The basic assumptions of the model are presented below. Grains of a poled ferroelectric perovskite-type ceramic with a tetragonal structure are assumed to be essentially composed of 90° domains (figure 25). 90° domains possess spontaneous polarization P_S and spontaneous strain, x_S. Elastic and electric fields will shift the domain wall by an amount Δl. Depending on the orientation of the field, certain domains will grow and others will shrink. The equation which describes the vibration of a domain wall is given by

$$m\Delta\ddot{l} + b\Delta\dot{l} + k\Delta l = -\left(\frac{\partial W_E}{\partial \Delta l} + \frac{\partial W_M}{\partial \Delta l}\right) \tag{66}$$

where m is the effective mass of the domain wall, b is the damping constant and k is the force constant, all per domain-wall unit area. The electric W_E and elastic W_M energy densities of the displaced wall are related to the driving electric and mechanical forces and wall displacement. If inertial ($m\Delta\ddot{l}$) effects in equation (66) are ignored, an expression

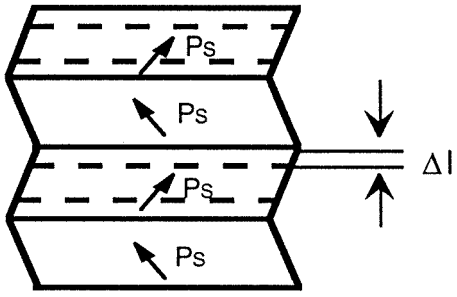

Figure 25. 90° domain walls in a cubic grain of a ferroelectric ceramic. Displacement of the walls by an external field applied parallel to the walls, in the plane of the drawing, is indicated by Δl, and polarization within each domain by P_S. The displaced walls are indicated by broken lines. (After [116].)

for domain-wall displacement Δl is found which depends on b, k, external fields E and X, spontaneous strain and polarization and geometrical factor f which determines the orientation of the walls. The displacement of the wall causes a contribution to the dielectric displacement, ΔD, and the total strain, Δx, of the sample, both of which are proportional to the wall displacement Δl. By integrating over all possible orientations of the domains it is possible to calculate the domain-wall contribution to the total electric displacement and strain and thus to the dielectric permittivity, elastic compliance and piezoelectric coefficients.

The calculations of material coefficients based on the model give a good agreement with experimental results and other phenomenological calculations. Detailed considerations [116] of the force constant k also showed that k is dependent on the domain width, and that it is stiffer for thin domains. These theoretical predictions are in agreement with recent experimental results [39, 105] which showed that domain-wall contributions to the piezoelectric effect in barium titanate ceramics are significantly weaker in fine-grained than in coarse-grained materials. The assumption of the model that 180° domain walls do not contribute to the dielectric permittivity, is consistent with experimental data used to verify the model. It seems to be, however, in disagreement with results of a recent experimental study which suggests a substantial contribution of 180° domain walls to the dielectric permittivity of soft PZT ceramics [36].

6.4.3. Freezing of domain-wall contributions at low temperatures. A reasonable and often-employed assumption in the description of domain-wall contributions to the properties of ferroelectric ceramics is that domain-wall movement is frozen at very low temperatures. The measured values of material coefficients at temperatures approaching 0 K should then correspond to values that are due only to the intrinsic lattice response. In doped materials in which doping affects mostly the extrinsic response, the effect of doping on the properties should therefore disappear at very low temperatures. This has indeed been observed in the case of the piezoelectric and dielectric properties of PZT ceramics containing various dopants but a similar Zr/Ti ratio [23, 140]. Even though the values of permittivities and piezoelectric coefficients of the examined samples are very different at room temperature, they converge to a common value at low temperatures as the domain-wall movement becomes gradually frozen (figure 26), [140].

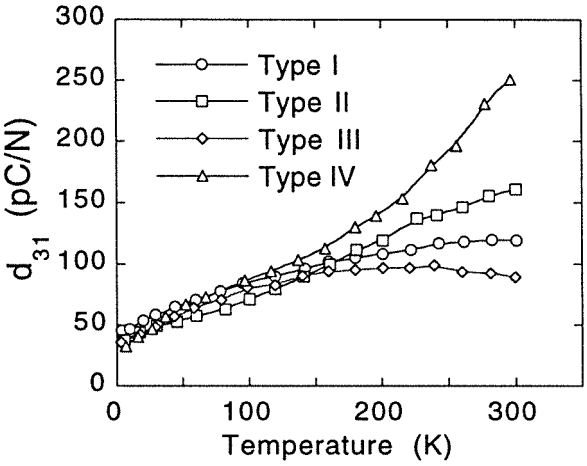

Figure 26. Temperature dependence of the longitudinal d_{33} piezoelectric coefficient for $Pb(Zr, Ti)O_3$ ceramics which have a similar Ti/Zr ratio but are doped with different dopants (Navy type I, II, III, IV). The difference in d_{33} at higher temperatures is due to different domain-wall contributions for ceramics with different dopants. At low temperatures, domain-wall contributions become 'frozen' and only the lattice contribution, which is similar for all examined ceramics, is present. (After [140].)

6.4.4. Field and frequency dependence of piezoelectric response. It has recently been shown that in several compositions of ferroelectric ceramics [38, 141] as well as in PZT ferroelectric thin films [142] the nonlinear direct piezoelectric effect at low to moderate driving fields may be described, in the first approximation, in terms of the Rayleigh relations. These relations were originally derived empirically by Rayleigh to describe the weak-field permeability and magnetization in ferromagnetic materials [143, 144] and were subsequently derived theoretically by Néel [145] who considered displacement of ferromagnetic domain walls in a magnetic field. Relations analogous to the magnetic case were later used to describe nonmagnetic processes, including polarization behaviour in a dipolar glass [146], contribution of displacement of ferroelectric domain walls to polarization and piezoelectric properties in ferroelectric single crystals [147], thin films [112] and ceramics [141]. The approach used may be summarized as follows, taking for example piezoelectric response of ferroelectric ceramics.

Displacement of domain walls is considered in a medium which contains randomly distributed defects which act as pinning centres for domain walls. In such a case the potential energy of the domain walls becomes an irregular function of the wall position, as shown in figure 27. Domain-wall displacement can now be expressed as a combination of a reversible movement around an equilibrium position (at the minimum of a potential well) and irreversible displacement across potential barriers, as shown in the figure 27. The irreversible displacement into a new equilibrium position occurs when the driving field is large enough to overcome potential barriers in the neighbourhood of the original position. Movement of domain walls in such a medium leads to field dependence of the piezoelectric charge and the piezoelectric coefficient, which can be expressed by the Rayleigh relations, given below for the direct piezoelectric coefficient d_{33} [38, 141]:

$$d_{33} = d_{\text{init}} + \alpha X_{\max} \tag{67}$$

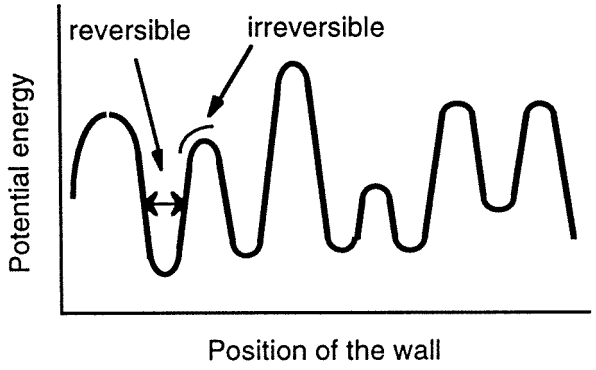

Figure 27. Potential of a domain wall in a medium with randomly distributed pinning centres.

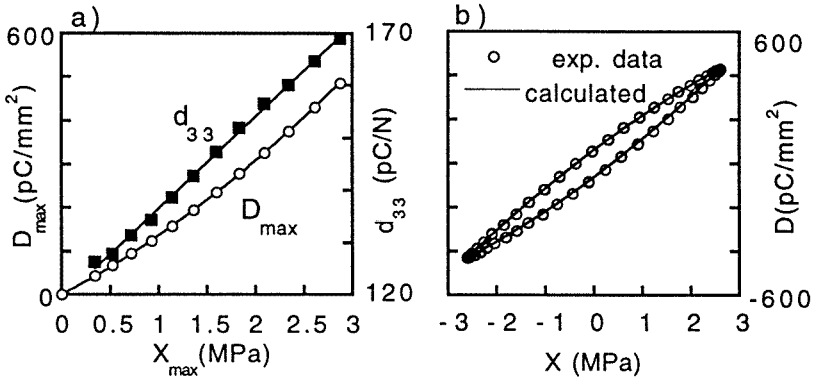

Figure 28. (*a*) Direct longitudinal piezoelectric coefficient d_{33} and piezoelectric charge amplitude D_{max} and (*b*) D–X hysteresis loop in a Nb-doped $Pb(Zr_{0.52}Ti_{0.48})O_3$ ceramic. Symbols represent experimental data. The full lines in (*a*) are fits of the data with equation (67) and with expression $D_{max} = d_{33}X_{max} = (d_{init} + \alpha X_{max})X_{max}$. The full line in (*b*) is calculated using equation (68) and the Rayleigh parameters obtained by fitting d_{33} (X_{max}). (See [38] for details.)

and

$$D(X) = (d_{init} + \alpha X_{max})X \pm \frac{\alpha}{2}(X_{max}^2 - X^2). \tag{68}$$

d_{init} is the so-called initial piezoelectric coefficient, X_{max} is the amplitude of the driving alternating pressure $X(t)$, $D(X)$ is the piezoelectric charge density and α is the Rayleigh coefficient. Equation (67) describes the field dependence of the piezoelectric coefficient d_{33} (figure 28(*a*)) whereas equation (68) describes the charge versus stress (or piezoelectric) hysteresis loop, which is obtained by cycling the driving pressure, as shown in figure 28(*b*). The piezoelectric coefficient is calculated as $d_{33} = D_{max}/X_{max}$ where D_{max} is the amplitude of the piezoelectric charge. The sign '+' in equation (68) corresponds to increasing and '−' to decreasing pressure. In the magnetic analogue, the piezoelectric coefficient corresponds to magnetic permeability, stress to magnetic field and charge to magnetization.

The piezoelectric hysteresis can be calculated for a given alternating field once the Rayleigh parameters d_{init} and α are known. These parameters can easily be determined experimentally by measuring d_{33} as a function of the driving field amplitude and using

equation (67). Figure 28 demonstrates the validity of the Rayleigh relationships in a $Pb(Zr, Ti)O_3$ ceramic by comparing experimentally determined d_{33} versus X_{max} and $D(X)$ versus X data with curves calculated using the Rayleigh equations (67) and (68). Piezoelectric hysteresis is a serious problem in applications of electromechanical actuators and sensors based on ferroelectric materials because it affects their precision. The description of piezoelectric properties in terms of the Rayleigh relationships is thus potentially a good starting point for modelling the response of ferroelectric-based electromechanical devices [38]. For practical purposes, if higher-order terms appear in (67), the expression for the hysteresis (68) may be easily modified to give a very good quantitative agreement with experimental data [38].

Rayleigh parameters are found to be strongly dependent on the grain size, local variations in composition and structure of the material, nature of defects, external bias fields, history of sample and ageing conditions. The analysis of the dielectric and piezoelectric properties in terms of the Rayleigh relations is thus a promising tool for describing the influence of various microstructural and structural parameters on the domain-wall displacement in ferroelectric materials [39]. It must be emphasized, however, that domain-wall pinning processes in ferroelectric materials can be very complex so that relatively simple model which results in the Rayleigh relations may not always adequately describe all observations. Nevertheless, a treatment of the piezoelectric and dielectric nonlinearities in terms of domain-wall pinning in random systems appears to be a promising general approach. Clearly, other types of domain-wall processes as well as other extrinsic contributions, can operate in ferroelectric materials [38] and may even dominate their piezoelectric and dielectric response.

In materials in which non-180° domain walls either do not exist or cannot contribute irreversibly to the piezoelectric response to applied fields, the Rayleigh coefficient α is zero and the piezoelectric coefficient is independent of the amplitude of the AC field. If there are no other piezoelectrically induced relaxational processes in the material (which for example may be due to point defects or reversible vibration of the domain walls), the piezoelectric response will also be hysteresis free. Such a piezoelectric response, seemingly free of extrinsic (and in particular, non-180° domain-wall) contributions, has indeed been observed in $SrBi_2Ti_2O_9$ and $SrBi_4Ti_4O_{15}$ [148] bismuth-based layer-structured ferroelectric (see section 4.8), as shown in figure 29 for $SrBi_2Ti_2O_9$. The complex domain-wall structure in monoclinic niobium-doped $Bi_4Ti_3O_{12}$ bismuth titanate, which also shows layered structure, leads to a nonlinear, frequency-dependent and hysteretic piezoelectric response (figure 29), but is has been shown that extrinsic contributions may be suppressed by doping the ceramics with large concentrations of Nb [149].

Studies of the frequency dependence of the piezoelectric coefficients in $Pb(Zr, Ti)O_3$ ceramics and thin films [142, 150, 151] show that the piezoelectric coefficients exhibit linear dependence on the logarithm of the driving field frequency (figure 30), again indicating that domain-wall pinning processes control the extrinsic piezoelectric response (cf figure 20).

Other types of frequency and field dependence of the piezoelectric coefficients have been observed in ferroelectric materials [53] including Debye-like relaxation in modified lead titanate ceramics [38].

6.4.5. Thin-film issues. There are several factors which obviously influence the piezoelectric response of ferroelectric thin films, including mechanical clamping to the substrate, orientation of the film, the level of polarization and breakdown field strength. Other effects, such as the influence of defects on the domain-wall contributions to the piezoelectric effect in thin films have not yet been studied in detail. Thus, it is presently

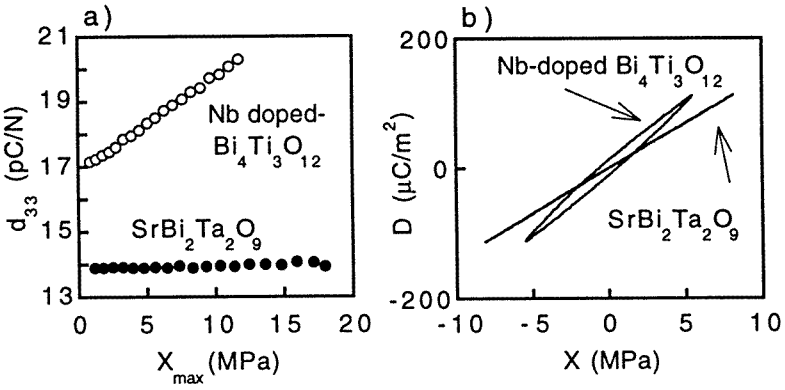

Figure 29. (*a*) Direct piezoelectric d_{33} coefficient for $SrBi_2Ta_2O_9$ and Nb-doped $Bi_4Ti_3O_{12}$ ceramics as a function of the amplitude X_{max} of the AC pressure. (*b*) Piezoelectric charge density, D, versus AC pressure, X, hysteresis for the two ceramics. Independence of the direct piezoelectric d_{33} coefficient in $SrBi_2Ta_2O_9$ ceramics of the driving field amplitude and the absence of charge-field hysteresis indicate that irreversible displacement of non-180° domain walls does not contribute to the piezoelectric response. In monoclinic Nb-doped bismuth titanate, a strong contribution from irreversible displacements of non-180° walls leads to the dependence of d_{33} on the field amplitude (*a*) and a large hysteresis (*b*). (For details see [38, 148, 149].)

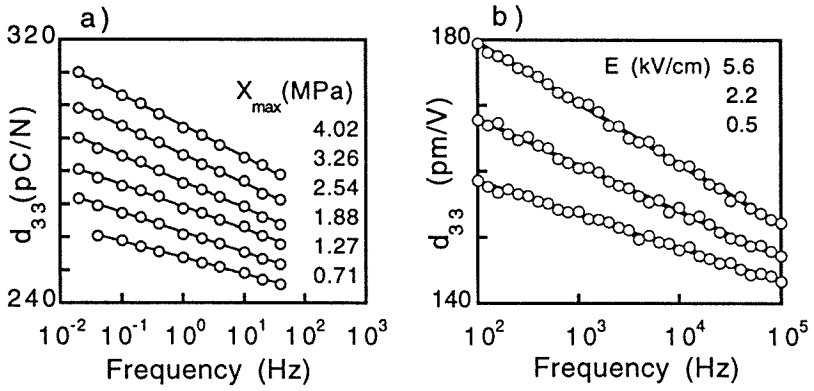

Figure 30. Frequency dependence of the longitudinal d_{33} piezoelectric coefficient for different amplitudes of driving fields: (*a*) Nb-doped $Pb(Zr_{0.52}Ti_{0.48})O_3$ ceramic (direct effect) and (*b*) 7.1 μm thick $Pb(Zr_{0.53}Ti_{0.47})O_3$ film (converse effect, effective coefficient, see section 6.4.5), cf figure 20. (Film data courtesy of A Kholkin.)

not clear whether, for example, the effect of acceptor and donor dopants on the properties of PZT films would lead to the same effects as in bulk materials.

Due to the clamping of the film to the substrate, measurements of the piezoelectric coefficients using the converse or direct effect take into account the stresses imposed on the film by the substrate. In the case of the converse piezoelectric effect, the effective piezoelectric coefficient may be easily calculated by using equation (27). Assume a polycrystalline film with randomly distributed grains which is poled along the z-axis (perpendicular to the plane of the substrate). For ideal clamping in the x–y plane (plane of the substrate) we have $x_1 = x_2 = 0$ and $x_3 \neq 0$. Due to the symmetry of the film in the plane of the substrate, $X_1 = X_2$, and because the surface of the film is free, $X_3 = 0$. Equation (27)

then gives [152] for the effective (measured) converse d_{33} in randomly oriented films (see the appendix for corresponding matrices):

$$(d_{33})_{\text{meas}} = d_{33} - 2d_{31}\frac{s_{13}^E}{(s_{11}^E + s_{12}^E)}. \tag{69}$$

Since in most materials $d_{31} < 0$, $s_{13} < 0$ and d_{31} is relatively large (in PZT d_{31} is roughly $\frac{1}{3}$ of d_{33}), the measured coefficient in films is always smaller than in unclamped materials. Similar relations can be derived for the direct effect [152]. Therefore, small reported values of the piezoelectric coefficients in films relative to the bulk ceramics values, can be at least partly explained by the clamping effects of the substrate. It is interesting to mention that in Ca-doped lead titanate thin films the piezoelectric coefficient is nearly equal to the values measured in ceramics [153]. This can be explained by the fact that the transverse piezoelectric coefficient in modified lead titanate is small [154] so that the correction term in equation (69) also becomes very small.

Good ferroelectric thin films usually posses a very high breakdown strength, and this allows the generation of electromechanical strains that are several times higher than in ceramics of similar compositions [23, 153, 155]. The strain–field butterfly loops in films are, however, often found to be highly asymmetrical even when no asymmetry was observed in the polarization loops. The origin of the asymmetry in the strain loops is not clear and a presence of residual substrate–film interfacial stresses has been suggested as a possible cause [155, 156].

7. Pyroelectric effect

7.1. Effects of electric field bias

The relationship (2) for the dielectric displacement may be written in polar materials as

$$D = \varepsilon_0 E + P + P_S = \varepsilon E + P_S. \tag{70}$$

By taking the derivative of equation (70) with respect to the temperature we obtain

$$p_i' = E_j \frac{\partial \varepsilon_{ij}}{\partial T} + p_i \tag{71}$$

where $p_i' = \partial D_i/\partial T$ is a generalized pyroelectric coefficient and p_i is defined by (7). It follows from equation (71) that even a nonpyroelectric material will show a pyroelectric-like response if it is biased by an electric field. From the symmetry point of view it is evident that the applied DC electric bias field and the crystal (even noncentrosymmetric) taken together possess a polar symmetry. In ferroelectric materials the electric bias field increases the transition temperature, reduces the dielectric permittivity and flattens its peak, and leads to a less abrupt decrease in polarization as the transition temperature is approached. A combination of these effects leads to a maximum in the pyroelectric responsivity at a certain field [2, 24, 106]. An additional beneficial effect of operation above T_C in ferroelectric materials (under DC bias) is that the loss associated with the displacement of domain walls is absent [24].

7.2. Clamped and free pyroelectric coefficient

Relation (26) with $E = 0$ and $X = 0$ gives the pyroelectric coefficient under constant (zero) stress conditions, when the sample is free to change its shape. This corresponds to the experimental conditions most frequently used for measurements of pyroelectric coefficients

in bulk materials. If the sample is, however, mechanically clamped, the change in the temperature will cause, through thermal expansion, stress in the sample which will then, through the direct piezoelectric effect, produce charge. This situation may be applied to pyroelectric thin films which are partially clamped in the plane of the substrate and free to expand in the thickness direction [157]. The relationship between the clamped and free pyroelectric coefficients may be obtained by considering equations (24) and (25) where thermal effects are included and by assuming zero electric field:

$$x = \alpha^{X,E}\Delta T + s^{T,E}X \tag{72}$$

$$D = p^{X,E}\Delta T + d^{T,E}X. \tag{73}$$

The tensor indices are omitted for simplicity. If the total strain x in equation (72) is zero, then the stress X which opposes the thermal strain is $X = -(\alpha^{X,E}/s^{T,E})\Delta T$. This stress induces charge through the piezoelectric effect. The total charge displacement due to the stress and temperature variation is obtained from equation (73) as

$$D = p^{X,E}\Delta T + d^{T,E}\left(-\frac{\alpha}{s^{T,E}}\right)\Delta T = (p^{X,E} - \alpha c^{T,E}d^{T,E})\Delta T = p^{x,E}\Delta T \tag{74}$$

where

$$p^{x,E} = p^{X,E} - \alpha c^{T,E}d^{T,E} \tag{75}$$

is the clamped (under constant or zero strain) pyroelectric coefficient. The p^x is sometimes called the primary or true pyroelectric coefficient. The term $\alpha c^{T,E}d^{T,E}$ which describes the contribution to the pyroelectric effect from the thermal expansion and piezoelectricity is called the secondary pyroelectric coefficient and may be comparable to the primary coefficient [1, 158]. A comparison of the values of primary and secondary pyroelectric coefficients for a large number of ferroelectrics may be found in [158]. Clamping to the substrate can, however, change the values of the intrinsic material parameters so that the piezoelectric coefficient in (75) may not be the same for the free crystal and the clamped film. A tertiary pyroelectric coefficient which is induced by the piezoelectric effect associated with strains caused by nonuniform heating of the sample may also be defined [1].

Appendix

The pyroelectric coefficient, dielectric permittivity, piezoelectric coefficient and elastic compliance matrices for poled ceramics and films with random orientation of grains have the same matrix elements as crystals which belong to the point group 6*mm* and are given below. Matrices for all other symmetries may be found in [6] (which includes noncrystallographic symmetries), [1, 2, 11]

$$(p) = \begin{pmatrix} 0 \\ 0 \\ p_3 \end{pmatrix} \qquad (\varepsilon) = \begin{pmatrix} \varepsilon_{11} & 0 & 0 \\ 0 & \varepsilon_{11} & 0 \\ 0 & 0 & \varepsilon_{33} \end{pmatrix}$$

$$(d_{\text{direct}}) = \begin{pmatrix} 0 & 0 & 0 & 0 & d_{15} & 0 \\ 0 & 0 & 0 & d_{15} & 0 & 0 \\ d_{31} & d_{31} & d_{33} & 0 & 0 & 0 \end{pmatrix}$$

$$(d_{\text{converse}}) = \begin{pmatrix} 0 & 0 & d_{31} \\ 0 & 0 & d_{31} \\ 0 & 0 & d_{33} \\ 0 & d_{15} & 0 \\ d_{15} & 0 & 0 \\ 0 & 0 & 0 \end{pmatrix} \qquad (s) = \begin{pmatrix} s_{11} & s_{12} & s_{13} & 0 & 0 & 0 \\ s_{12} & s_{11} & s_{13} & 0 & 0 & 0 \\ s_{13} & s_{13} & s_{33} & 0 & 0 & 0 \\ 0 & 0 & 0 & s_{44} & 0 & 0 \\ 0 & 0 & 0 & & s_{44} & 0 \\ 0 & 0 & 0 & 0 & 0 & 2(s_{11} - s_{12}) \end{pmatrix}.$$

References

[1] Nye J F 1985 *Physical Properties of Crystals* (Oxford: Oxford University Press)
[2] Lines M E and Glass A M 1979 *Principles and Applications of Ferroelectrics and Related Materials* (Oxford: Clarendon)
[3] Mitsui T, Tatsuzaki I and Nakamura E 1976 *An Introduction to the Physics of Ferroelectrics* (London: Gordon and Breach)
[4] Newnham R E 1990 *Proc. Chemistry of Electronic Ceramic Materials (National Institute of Standards and Technology, Jackson, WY)* Special Publication 804
[5] Kuwata J, Uchino K and Nomura S 1980 *Japan. J. Appl. Phys.* **19** 2099
[6] Sirotin Y I and Shaskolskaya M P 1982 *Fundamentals of Crystal Physics* (Moscow: Mir)
[7] Fox G R, Damjanovic D, Danai P A, Setter N, Limberger H G and Ky N H 1995 *Mater. Res. Soc. Symp. Proc.* **360** 389
[8] Surowiak Z, Margolin A M, Zakharchenko I N and Biryukov S V 1989 *Thin Solid Films* **176** 227
[9] Kanno I, Fujii S, Kamada T and Takayama R 1997 *Appl. Phys. Lett.* **70** 1378
[10] Reichl L E 1980 *A Modern Course in Statistical Physics* (London: Edward Arnold)
[11] Xu Y 1991 *Ferroelectric Materials and Their Applications* (Amsterdam: North-Holland)
[12] Park S E and Shrout T R 1997 *J. Appl. Phys.* **82** 1804
[13] Joan F and Shirane G 1962 *Ferroelectric Crystals* (New York: Pergamon)
[14] Haun M J, Furman E, Jang S J, McKinstry H A and Cross L E 1987 *J. Appl. Phys.* **62** 3331
[15] Haun M J, Zhuang Z Q, Furman E, Jang S J and Cross L E 1989 *J. Am. Ceram. Soc.* **72** 1140
[16] Nelmes R J and Kuhs W F 1985 *Solid State Commun.* **54** 721
[17] Stemmer S, Streiffer S K, Ernst F and Rühle M 1995 *Phil. Mag.* A **71** 713
[18] Burfoot J C and Taylor G W 1979 *Polar Dielectrics and Their Applications* (London: Macmillan)
[19] Arlt G 1990 *J. Mater. Sci.* **25** 2655
[20] Newnham R E 1975 *Structure–Property Relations* (Berlin: Springer)
[21] Shur V Y 1996 Fast polarization reversal process: evolution of ferroelectric domain structure in thin films *Ferroelectric Thin Films: Synthesis and Basic Properties* ed C P de Araujo, J F Scott and G W Taylor (Amsterdam: Gordon and Breach) p 153
[22] Fousek J and Janovec V 1969 *J. Appl. Phys.* **40** 135
[23] Cross L E 1993 Ferroelectric ceramics: tailoring properties for specific applications *Ferroelectric Ceramics* ed N Setter and E L Colla (Basel: Birkhäuser) p 1
[24] Whatmore R W 1986 *Rep. Prog. Phys.* **49** 1335
[25] Sawyer C B and Tower C H 1930 *Phys. Rev.* **35** 269
[26] Ishibashi Y 1996 Polarization reversal in ferroelectrics *Ferroelectric Thin Films: Synthesis and Basic Properties* ed C P de Araujo, J F Scott and G W Taylor (Amsterdam: Gordon and Breach) p 135
[27] Shur V and Rumyantsev E 1988 *J. Korean Phys. Soc.* **32** S727
[28] Scott J F, Kammerdiner L, Parris M, Traynor S, Ottenbacher V, Shawabkeh A and Oliver W F 1988 *J. Appl. Phys.* **64** 787
[29] Ishibashi Y and Takagi Y 1971 *J. Phys. Soc. Japan* **31** 506
[30] Caspari M E and Merz W J 1950 *Phys. Rev.* **80** 1082
[31] Jaffe B, Cook W R and Jaffe H 1971 *Piezoelectric Ceramics* (New York: Academic)
[32] Tsurumi T, Kumano Y, Ohashi N, Takenaka T and Fukunaga O 1997 *Japan. J. Appl. Phys.* **36** 5970
[33] Zipparo M J, Shung K K and Shrout T R 1997 *IEEE Trans. UFFC* **44** 1038
[34] Uchino K 1986 *Am. Ceram. Soc. Bull.* **65** 647
[35] Zhang Q M, Pan W Y, Jang S J and Cross L E 1988 *J. Appl. Phys.* **64** 6445
[36] Zhang Q M, Wang H, Kim N and Cross L E 1994 *J. Appl. Phys.* **75** 454
[37] Hagemann H 1978 *J. Phys. C: Solid State Phys.* **11** 3333
[38] Damjanovic D 1997 *J. Appl. Phys.* **82** 1788
[39] Damjanovic D and Demartin M 1997 *J. Phys.: Condens. Matter* **9** 4943
[40] Bondarenko E I, Topolov V Y and Turik A V 1991 *Ferroelectr. Lett.* **13** 13
[41] Carl K and Haerdtl K H 1978 *Ferroelectrics* **17** 473
[42] Salje E K H 1990 *Phase Transitions in Ferroelectric and Co-elastic Crystals* (Cambridge: Cambridge University Press)
[43] Dvorak V 1974 *Ferroelectrics* **27** 1
[44] Maugin G A, Pouget J, Drouot R and Collet B 1992 *Nonlinear Electromechanical Couplings* (Chichester: Wiley)
[45] Devonshire A F 1949 *Phil. Mag.* **40** 1040

[46] Haun M J, Furman E, Jang S J and Cross L E 1989 *Ferroelectrics* **99** 63
[47] Cross L E 1972 Thermodynamic phenomenology of ferroelectricity in single crystal and ceramic systems *Physics of Electronic Ceramics* Part B, ed L L Hench and D B Dove (New York: Dekker) p 707
[48] Haun M J, Furman E, Jang S J and Cross L E 1989 *IEEE Trans. UFFC* **36** 393
[49] Wersing W, Lubitz K and Mohaupt J 1989 *IEEE Trans. UFFC* **36** 424
[50] Marutake M 1956 *J. Phys. Soc. Japan* **11** 807
[51] Turik A V, Fesenko E G, Gavrilyatchenko V G and Khasabova G I 1975 *Sov. Phys. Crystallogr.* **19** 677
[52] Arlt G, Dederichs H and Herbeit R 1987 *Ferroelectrics* **74** 37
[53] Hamano K and Yamaguchi T 1982 *Ferroelectrics* **42** 23
[54] Tilley D R 1993 *Phase Transitions in Thin Films in Ferroelectric Ceramics* ed N Setter and E Colla (Basel: Birkhaüser) p 163
[55] Qu B-D, Zhong W-L and Zhang P-L 1994 *J. Phys.: Condens. Matter* **6** 1207
[56] Brennan C J 1992 *Mater. Res. Soc. Symp. Proc.* **243** 141
[57] Arlt G and Neumann H 1988 *Ferroelectrics* **87** 109
[58] Desu S B, Dudkevich V P, Dudkevich V P, Zakharchenko I N and Kushlyan G L 1996 *Mater. Res. Soc. Proc.* **401** 195
[59] Pertsev N A, Zembilgotov A G and Tagantsev A K 1998 *Phys. Rev. Lett.* **80** 1988
[60] Cochran W 1960 *Adv. Phys.* **9** 387
[61] Cohen R E (ed) 1996 *Ferroelectrics* **194** 1–343
[62] Saghi-Szabo G and Cohen R E 1997 *Ferroelectrics* **194** 287
[63] Subbarao E C 1962 *J. Phys. Chem. Solids* **23** 665
[64] Takenaka T, Sakata K and Toda K 1985 *Japan. J. Appl. Phys.* **24** 730
[65] Withers R L, Thompson J G and Rae A D 1991 *J. Solid State Chem* **94** 404
[66] Megaw H D 1957 *Ferroelectricity in Crystals* (London: Methuen)
[67] Tomashpolski Y Y, Sevostianov M A, Pentegova M V, Srokina L A and Venevtsev Y N 1974 *Ferroelectrics* **7** 257
[68] Tagantsev A K 1996 *Ferroelectrics* **184** 79
[69] Tagantsev A K 1997 *Integr. Ferroelectr.* **16** 237
[70] Lebedev N I and Sigov A S 1994 *Integr. Ferroelectr.* **4** 21
[71] Waser R and Klee M 1992 *Integr. Ferroelectr.* **2** 23
[72] Fridkin B M 1980 *Ferroelectric Semiconductors* (New York: Consultants Bureau)
[73] Herbert J M 1985 *Ceramic Dielectrics and Capacitors* (New York: Gordon and Breach)
[74] Shur M 1990 *Physics of Semiconductor Devices* (Englewood Cliffs, NJ: Prentice-Hall)
[75] Tagantsev A K, Landivar M, Colla E, Brooks K G and Setter N 1995 Depletion, depolarizing effects and switching in ferroelectric thin films *Science and Technology of Electroceramic Thin Films* ed O Auciello and R Waser (Boston, MA: Kluwer) p 301
[76] Waser R 1997 *Integr. Ferroelectr.* **15** 39
[77] Tagantsev A K, Landivar M, Colla E and Setter N 1995 *J. Appl. Phys.* **78** 2623
[78] Robels U, Calderwood J H and Arlt G 1995 *J. Appl. Phys.* **77** 4002
[79] Miller S L, Nasby J R, Schwank J R, Rodgers M S and Dressendorfer P V 1990 *J. Appl. Phys.* **68** 6463
[80] Jiang Q Y, Subbarao E C and Cross L E 1994 *J. Appl. Phys.* **75** 7433
[81] Jiang Q, Subbarao E C and Cross L E 1994 *Ferroelectrics* **154** 119
[82] Jiang Q Y, Cao W and Cross L E 1994 *J. Am. Ceram. Soc.* **77** 211
[83] Paz de Araujo C A, Cuchiaro J D, McMillan L D, Scott M C and Scott J F 1995 *Nature* **374** 627
[84] Ramesh R, Chan W K, Wilkens B, Gilchrist H, Sands T, Tarascon J M, Ford D K, Lee J and Safari A 1992 *Appl. Phys. Lett.* **61** 1537
[85] Al-Shareef H N, Dimos D, Warren W L and Tuttle B A 1997 *Integr. Ferroelectr.* **15** 53
[86] Warren W L, Dimos D, Tuttle B A, Pike G E, Schwartz R W, Clews P J and McIntyre D C 1995 *J. Appl. Phys.* **77** 6695
[87] Johnson D J, Amm D T, Griswold E, Sreenivas K, Yi G and Sayer M 1990 *Mater. Res. Soc. Symp. Proc.* **200** 289
[88] Duiker H M, Beale P D, Scott J F, Paz de Araujo C A, Melnick B M, Cuchiaro J D and McMillan L D 1990 *J. Appl. Phys.* **68** 5783
[89] Scott J F, Paz de Araujo C A, Melnick B M, McMillan L D and Zuleeg R 1991 *J. Appl. Phys.* **70** 382
[90] Yoo I K and Desu S B 1992 *Phys. Status Solidi* a **133** 565
[91] Pan W Y, Yei C F and Tuttle B A 1992 Ferroelectric fatigue in modified bulk lead zirconate titanate ceramics and thin films *Ceramic Transactions: Ferroelectric films* ed A S Bhalla and K M Nair (Westerville, OH: The American Ceramic Society) p 385

[92] Colla E L, Taylor D V, Tagantsev A K and Setter N 1998 *Appl. Phys. Lett.* **72** 2478
[93] Colla E L, Tagantsev A K, Taylor D V and Kholkin A L 1998 *J. Korean Phys. Soc.* **32** S1353
[94] Mihara T, Watanabe H and Paz de Araujo C A 1994 *Japan. J. Appl. Phys.* **33** 5281
[95] Warren W L, Tuttle B A and Dimos D 1995 *Appl. Phys. Lett.* **67** 1426
[96] Anderson J R, Brady G W, Merz W J and Remeika J P 1955 *J. Appl. Phys.* **26** 1387
[97] Warren W L, Dimos D, Tuttle B A, Nasby R D and Pike G E 1994 *Appl. Phys. Lett.* **65** 1018
[98] Colla E L, Tagantsev A K, Taylor D V and Kholkin A L 1997 *Integr. Ferroelectr.* **18** 19
[99] Colla E L, Kholkin A L, Taylor D, Tagantsev A K, Brooks K G and Setter N 1995 *Microelectron. Eng.* **29** 145
[100] Colla E L, Taylor D V, Tagantsev A K and Setter N 1998 *Appl. Phys. Lett.* **72** 2763
[101] Tagantsev A K 1997 Personal communication
[102] Syrowiak Z, Nikitin Y S, Svirdov E V, Mukhortov V M and Dudkevich V P 1991 *Izv. Akad. Nauk SSSR, Ser. Fiz.* **55** 500
[103] Rossetti G A, Cross L E and Kushida K 1991 *Appl. Phys. Lett.* **59** 2524
[104] Shepard J F, Trolier-McKinstry S, Hendrickson M A and Zeto R 1996 *Proc. 10th IEEE Int. Symp. on Applications of Ferroelectrics* vol I, ed B M Kilwicki, A Amin and A Safari (Piscataway, NJ: IEEE Service Center) p 161
[105] Demartin M and Damjanovic D 1996 *Appl. Phys. Lett.* **68** 3046
[106] Herbert J M 1982 *Ferroelectric Transducers and Sensors* (New York: Gordon and Breach)
[107] Wouters D J, Willems G, Lee E-G and Maes H E 1997 *Integr. Ferroelectr.* **15** 79
[108] Bar-Chaim N, Brunstein M, Grünberg J and Seidman A 1974 *J. Appl. Phys.* **45** 2398
[109] Eatough M O, Dimos D, Tuttle B A, Warren W L and Ramesh R 1995 *Mater. Res. Soc. Symp. Proc.* **361** 111
[110] Tuttle B A, Garino T J, Voigt J A, Headley T J, Dimos D and Eatough M O 1995 Relationships between ferroelectric 90° domain formation and electrical properties of chemically prepared Pb(Zr, Ti)O3 thin films *Science and Technology of Electroceramic Thin Films* ed O Auciello and R Waser (Dordrecht: Kluwer) p 117
[111] Hector J, Floquet N, Niepce J C, Gaucher P and Ganne J P 1995 *Microelectron. Eng.* **29** 285
[112] Taylor D V and Damjanovic D 1997 *J. Appl. Phys.* **82** 1973
[113] Buessem W R, Cross L E and Goswami A K 1966 *J. Am. Ceram. Soc.* **49** 33
[114] Bell A J 1994 *Proc. 9th IEEE Int. Symp. on Application of Ferroelectrics* (Piscataway, NJ: IEEE Service Center)
[115] Arlt G, Henning D and de With G 1985 *J. Appl. Phys.* **58** 1619
[116] Arlt G and Pertsev N A 1991 *J. Appl. Phys.* **70** 2283
[117] Bernaben N, Leriche A, Thierry B, Niepce J C and Waser R 1994 *Proc. Electroceramics* vol IV, ed R Waser, S Hoffman, D Bonnenberg and C Hoffmann (Aachen: RWTH) p 105
[118] Hayashi T 1994 *Japan. J. Appl. Phys.* **33** 5278
[119] Demartin M 1996 *PhD Thesis* Swiss Federal Institute of Technology—EPFL, Lasuanne, Switzerland
[120] Cao W and Randall C A 1996 *J. Phys. Chem. Solids* **57** 1499
[121] Herbeit R, Tenbrock H and Arlt G 1987 *Ferroelectrics* **76** 319
[122] Robels U and Arlt G 1993 *J. Appl. Phys.* **73** 3454
[123] Warren W L, Pike G E, Vanheusden K, Dimos D, Tuttle B A and Robertson J 1996 *J. Appl. Phys.* **79** 9250
[124] Teowee G, Boulton J M, Lee S C and Uhlmann D R 1992 *Mater. Res. Soc. Symp. Proc.* **243** 255
[125] Kholkin A L, Tagantsev A K, Colla E L, Taylor D V and Setter N 1997 *Integr. Ferroelectr.* **15** 317
[126] Pike G E, Warren W L, Dimos D, Tuttle B A, Ramesh R, Lee J, Keramidas V G and Evans J T Jr 1995 *Appl. Phys. Lett.* **66** 484
[127] Lee E-G, Wouters D J, Willems G and H E M 1997 *Integr. Ferroelectr.* **16** 165
[128] Haertling G H 1992 Current status of thin/thick film ferroelectrics *Ferroelectric Films* vol 25, ed A S Bhalla and K M Nair (Westerville, OH: The American Ceramic Society)
[129] Benedetto J M 1997 *Integr. Ferroelectr.* **15** 29
[130] Helwege K H and Helwegge A M 1981 *Ferroelectrics and Related Substances (Landolt–Boernstein Series 16)* (Berlin: Springer)
[131] Foster C M, Bai G-R, Csencsits R, Vetrone J, Jammy R, Wills L A, Carr E and Amano J 1997 *J. Appl. Phys.* **81** 2349
[132] Chen H D, Udayakumar K R, Gaskey C J and Cross L E 1995 *Appl. Phys. Lett.* **67** 3411
[133] Carl K and Hardtl K H 1971 *Phys. Status Solidi* A **8** 87
[134] Mishra S K, Pandey D and Singh A P 1996 *Appl. Phys. Lett.* **69** 1707
[135] Lambeck P V and Jonker G H 1978 *Ferroelectrics* **22** 729

[136] Nowick A S and Heller W R 1965 *Adv. Phys.* **14** 101
[137] Arlt G 1982 *Ferroelectrics* **40** 149
[138] 1989 *Ferroelectrics* **98** pp 3–303 (Special issue on domain structures in ferroelectrics, ferroelastics, and other ferroic materials)
[139] Herbeit R, Robels U, Dederichs H and Arlt G 1989 *Ferroelectrics* **98** 107
[140] Zhang X L, Chen Z X, Cross L E and Schulze W A 1983 *J. Mater. Sci* **18** 968
[141] Damjanovic D and Demartin M 1996 *J. Phys. D: Appl. Phys.* **29** 2057
[142] Damjanovic D, Taylor D V, Kholkin A L, Demartin M, Brooks K G and Setter N 1997 *Mater. Res. Soc. Proc.* **459** 15
[143] Lord Rayleigh R S 1887 *Phil. Mag.* **23** 225
[144] Jiles D 1991 *Introduction to Magnetism and Magnetic Materials* (London: Chapman and Hall)
[145] Néel L 1942 *Cah. Phys.* **12** 1
[146] Lyons, K B, Fleury P A, Negran T J and Carter H L 1987 *Phys. Rev.* B **36** 2465
[147] Shil'nikov A V, Galiyarova N M, Gorin S V, Vasil'ev D G and Vologirova L K 1991 *Izv. Akad. Nauk SSSR, Ser. Fiz.* **55** 578
[148] Reaney I M and Damjanovic D 1996 *J. Appl. Phys.* **80** 4223
[149] Damjanovic D, Demartin M, Shulman H S, Testorf M and Setter N 1996 *Sens. Actuators* A **53** 353
[150] Damjanovic D 197 *Phys. Rev.* B **55** R649
[151] Pérez-Enciso E, Agraït N and Vieira S 1997 *Phys. Rev.* B **56** 2900
[152] Lefki K and Dormans G J M 1994 *J. Appl. Phys.* **76** 1764
[153] Kholkin A L, Calzada M L, Ramos P, Mendiola J and Setter N 1996 *Appl. Phys. Lett.* **69** 3602
[154] Damjanovic D, Gururaja T R and Cross L E 1987 *Am. Ceram. Soc. Bull.* **66** 699
[155] Li J-F, Viehland D D, Tani T, Lakeman C D E and Payne D A 1994 *J. Appl. Phys.* **75** 442
[156] Li J-F, Viehland D, Lakeman C D E and Payne D A 1995 *J. Mater. Res.* **10** 1435
[157] Zook J D and Liu S T 1978 *J. Appl. Phys.* **49** 4604
[158] Bhalla A S and Cross L E 1981 *Ferroelectrics* **38** 935
[159] Tagantsev A K, Pawlaczyk C, Brooks K and Setter N 1994 *Integr. Ferroelectr.* **4** 1